Electronic Materials Letters, Vol. 9, No. 2 (2013), pp. 133-153
DOI: 10.1007/s13391-012-2134-7

Review Paper

Graphene Composites as Anode Materials in Lithium-Ion Batteries

M. Mazar Atabaki* and R. Kovacevic

Research Center for Advanced Manufacturing (RCAM), Department of Mechanical Engineering, Southern Methodist University, 3101 Dyer Street, Dallas, TX 75205, USA

Since the world of mobile phones and laptops has significantly altered by a big designer named Steve Jobs, the electronic industries have strived to prepare smaller, thinner and lower weight products. The giant electronic companies, therefore, compete in developing more efficient hardware such as batteries used inside the small metallic or polymeric frame. One of the most important materials in the production lines is the lithium-based batteries which is so famous for its ability in recharging as many times as a user needs. However, this is not an indication of being long lasted, as many of the electronic devices are frequently being used for a long time. The performance, chemistry, safety and above all cost of the lithium ion batteries should be considered when the design of the compounds are at the top concern of the engineers. To increase the efficiency of the batteries a combination of graphene and nanoparticles is recently introduced and it has shown to have enormous technological effect in enhancing the durability of the batteries. However, due to very high electronic conductivity, these materials can be thought of as preparing the anode electrode in the lithium-ion battery. In this paper, the various approaches to characterize different types of graphene/nanoparticles and the process of preparing the anode for the lithium-ion batteries as well as their electrical properties are discussed.

Keywords: lithium ion battery, graphene, anode materials

1. INTRODUCTION

Lithium ion batteries were first proposed in the 1969 by Whittingham and commercially developed in the 1990's. Since then, there were a lot of improvements in the design of the materials inside the variety of small boxes. In the lithium batteries, lithium ions move from the negative electrode to the positive electrode during discharge, and back when charging. The electrodes of a lithium-ion battery are made of lightweight lithium and carbon. Lithium is also a highly reactive element, meaning that a lot of energy can be stored in its atomic bonds. This interprets into a very high energy density for lithium-ion batteries. Conventional batteries based on intercalation chemistry have a limitation with respect to increasing the battery energy density, as a result of topotactic redox reactions. Their maximum energy densities are not sufficient to meet the demands of new markets such as electric vehicles. Lithium ion batteries also exhibit high energy density values but suffer from poor power densities.[1] Therefore, new electrochemical systems with higher energy density can be introduced for next-generation batteries.[2] Graphene, as a miracle material, is chemically stable and has high electrical conductivity and it can move electrons easily, so it can be considered as a suitable anode alternative for the battery applications. Improved anodes also allow for storage of more lithium ions, which can increase the battery's capacity and give laptops, tablets, mobile phones, electric vehicles and renewable sources of energy longer battery life. Batteries with graphene can also last significantly longer than conventional batteries. The coating of the lithium-ion batteries can swell and flex without mechanical breakdown, which gives them a significantly longer cycle life in a battery, in some cases up to ten times longer. By comparison, as lithium ions are inserted and removed from electrode material in a typical battery, the material swells and shrinks, leading to a quick breakdown. The efficient conductivity of graphene also leads to less resistive heating within the electrode, so batteries can operate at lower temperatures, which adds to the battery safety. Lithium ions load in the battery materials very fast, remaining to get in the electrode material. This generates an over-voltage situation that can result in overheating, and short circuits that have caused fires in several types of lithium-ion batteries. Therefore, the manufacturers deliberately limit the rate of charge and discharge to very low levels to keep the batteries in a stable operating regime. This study is intended to investigate the recent developments in using graphene and graphene-like composites for the utilization as an anode material in the lithium-ion batteries.

*Corresponding author: mmazaratabak@smu.edu

2. EXPERIMENTAL PROCEDURE

Graphene has many advantages if it is used in the anodes. These include superior electrical conductivity, high surface area as the theoretical specific surface area of monolayer graphene is 2620 m^2g^{-1}, a high surface-to-volume ratio, ultra-thin thickness which can shortens the diffusion distance of ions, structural flexibility that paves the way for constructing flexible electrodes, thermal and chemical stability which guarantee its use in harsh environments, abundant surface functional groups which make it hydrophilic in aqueous electrolytes, and provide binding sites with other atoms or functional groups, a broad electrochemical window that is critical for increasing energy density and being one of the lowest cost material for mass production.[3,4] It is highly believed that computation, mathematical modeling and simulation will be the key to better achievements in designing of high-energy and high-power devices. The binding force between the graphene sheets is for weak Van der Waals interactions. It is believed that during the lithium intercalation, the lithium valence electrons and graphite interlayer hybridize; so understanding the interactions in this system is very important. The structural energies of this interaction have been predicted.[5] Graphite compounds have theoretical capacity of around 372 $mAhg^{-1}$ as a result of the formation of LiC_6.[6-9]

$$Li + 6C + e^- \leftrightarrow LiC_6. \quad (1)$$

The diffusion coefficient of lithium ions can be predicted by cyclic voltammetry technique and Randles-Sevcik equation.[10]

$$i_p = 0.4463nFAC\left(\frac{nFVD}{RT}\right)^{0.5} \xrightarrow{RoomTemperature}$$

$$i_p = kn^{3/2}V^{1/2}D^{1/2}AC \quad (2)$$

where n is the number of charges involved in the electrochemical half-reaction, F is Faraday's constant (96.485 C mol^{-1}), A is the area of the electrode, C is the molar concentration of Li^+ in the electrolyte, V is the voltage sweep rate (Vs^{-1}), D is the diffusion coefficient of lithium ions ($cm^2\ s^{-1}$), R is the universal gas constant (8.314 J $mol^{-1}\ K^{-1}$), T is the absolute temperature (K), and k is a constant equal to 2.69×10^5 C $mol^{-1}V^{-1/2}$. So, the diffusion coefficient of Li^+ can be predicted by:

$$D_{Li^+} = \left(\frac{m}{Kn^{3/2}AC}\right)^2 \quad (3)$$

where m is the slope of peak current for different scan rates in a linear graph from Eq. (2). In very oriented pyrolytic graphite, the diffusion coefficient of Li^+ in the direction parallel to the graphene plane is 4.4×10^{-6} cm^2s^{-1}[11] and based on the diffusivity of lithium ions in graghene the charge and discharge is high sufficient to develop the power. To explain the thermodynamical behavior of the lithium and graphene interaction, a cluster-expansion method has been presented at finite temperature.[12] The energy of structure is given by:

$$E_v^{predict} = C + \sum_i V\sigma_i + \sum_{ij} V^{ij}\sigma_i\sigma_j + \ldots \quad (4)$$

where $E_v^{predict}$ is the energy of structure v, C is a constant and V^{ij} is cluster interaction in sites i and j. However, the energy of formation of the compounds can be predicted by:

$$E_{compound}(Li_xC_6) = E(Li_xC_6) - E_{graphite}(C_6) - xE_{Li}(Li)\ . \quad (5)$$

Grand canonical and canonical Monte Carlo simulations based on the METROPOLIS algorithm, using Fick's second law of diffusion, can be employed for the cluster expansions in order to calculate the changes in the phase diagram.

$$D_C = \lim_{i\to\infty}\left[\frac{1}{2dt}\times\left(\frac{1}{N}\times\left(\sum_{i=1}^{N}\vec{r}_i(t)\right)\right)\right]\times\left(\frac{\partial\left(\frac{\mu}{k_BT}\right)}{k_BT\times\partial\ln x}\right) \quad (6)$$

where D_C is the intrinsic diffusion coefficient, $\vec{r}_i$ is the displacement of ith lithium ion after time (t), N is the number of diffused lithium ions and d is the dimension of the diffusion network. $\vec{r}_i$ can be kinetically calculated in Monte Carlo simulations. In addition, the frequency of lithium ions movement to the neighboring sites can be estimated.

$$\Gamma = \nu^* \exp\left(\frac{-\Delta E_k}{k_BT}\right) \quad (7)$$

where E_k is the difference between the energy at an activated state and the initial equilibrium state and v is an effective vibrational frequency. Figure 1 shows the first principle Mont Carlo calculation of phase diagram for the lithium-graphene binary system. The simulation confirmed intraplanar diffusion of lithium at the edges of graphene structure as it is faster than defect-induced interlayer diffusion through the basal planes.

Multiwall carbon nanotubes prepared by layer-by-layer technique are recently introduced as anode materials having a density of about 100 $kWkg^{-1}$ are one of those that can be nominated as the future of the anodes.[13] As the presence of carbon nanotubes indicated a new entrance for the development of more efficient anodes in the lithium ion batteries, graphene began its domination for the next generation of the lithium ion batteries by forming Li_2C_6 composition during the interaction with the lithium ions.[14,15] However, using graphene alone as an anode material might cause significant drawbacks in the transportation of the lithium ions, limiting its application in the sizable batteries. With applying physical vapor deposition technique, the carbon films can be homogeneously deposited on the anodes and make them more

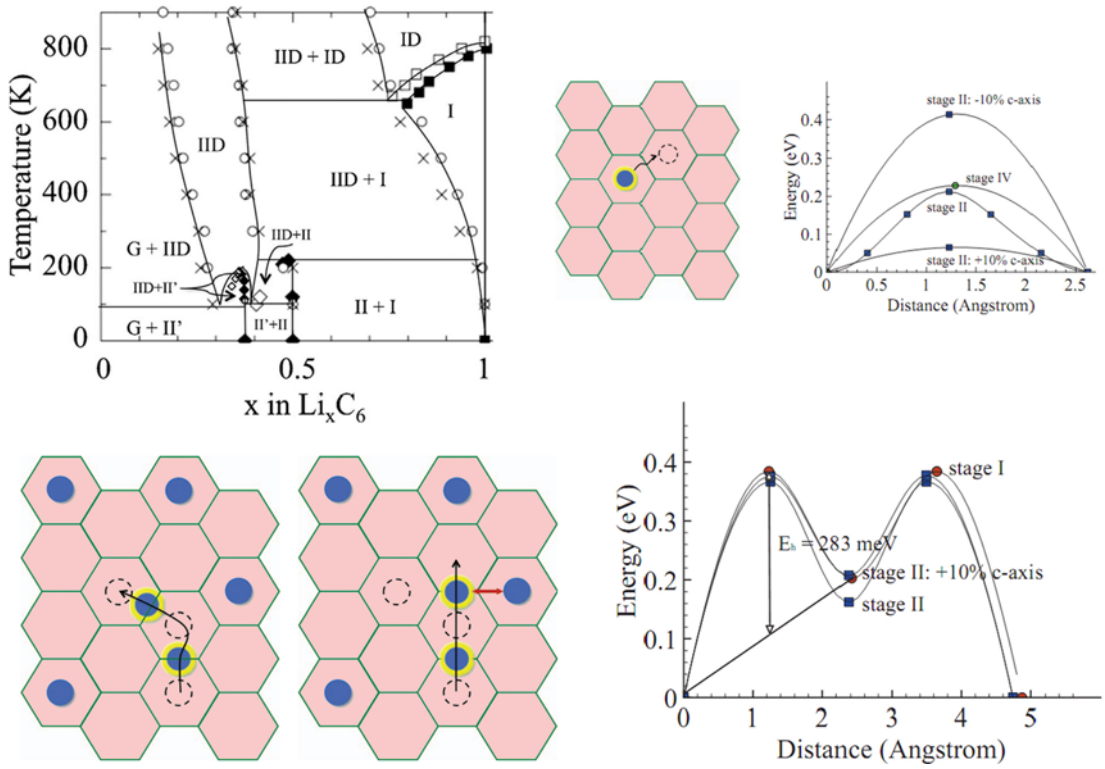

Fig. 1. First-principles phase diagram and energy barriers obtained from Monte Carlo simulations in stages I and II of cluster expansion.[12]

efficient in terms of storage space and reduces the formation of solid electrolyte interphase, reaching to intial capacity of 987 $mAhg^{-1}$ and coulombic efficiency of 82%.[16] It is, however, partial diffusion of lithium ions in the deposited carbon films causes low capacities in higher rates. Therefore, there are many researches and funding projects to develop alternative materials for this loss of capacities and among Al, Sn, Ge and Si materials, those combinations with graphene are much of the interest of research communities and industries. For example, when Al was used as the anode, the lithium ions showed very low diffusion as the diffusion coefficient of lithium ions in aluminium is 6×10^{-12} cm^2s^{-1}. On the other hand, when Al reacts with the Li three intermetallics can be formed (AlLi, Al_2Li_3 and Al_4Li_9). AlLi can deliver a capacity of 993 $mAhg^{-1}$ and Al_4Li_9 can exhibit higher capacity of about 2234 $mAhg^{-1}$ as it has lower weight. As Al is a metal with high expansion in its volume, leading to pulverization, cracks formation, delamination and loss in electrical contact, its usage in the lithium ion batteries as an anode is rather limited.[17] Tin also has the similar problem as the diffusivity of lithium ions in tin is significantly high at 5.9×10^{-7} cm^{2-1} which allows for rapid charge/discharge cycles[18] and volume expansion of tin is around 300%. The theoretical capacity of germanium is reported to be 1600 $mAhg^{-1}$ while that of silicon is stated to be 4200 $mAhg^{-1}$, more than ten times increase from the theoretical capacities of graphite anodes. Germanium has three step electro-chemical reaction during its initial charge cycle (see Eq. (8)). The formation of $Li_{15}Ge_4$ and $Li_{22}Ge_5$ intermetallics causes a volume expansion of 270%, which is again another weak point for the abovementioned elements.

$$Ge \rightarrow Li_9Ge_4 \rightarrow Li_7Ge_2 \rightarrow Li_{12}Ge_4 + Li_{22}Ge_5. \quad (8)$$

Silicone with theoretical capacity of 4200 $mAhg^{-1}$ is another alternative material as it reacts with lithium and forms $Li_{22}Si_5$ intermetallic.

$$22Li^+ + 5Si + 22e^- \rightarrow Li_{22}Si_5. \quad (9)$$

However, this element as well as other elements used as the anode material has many drawbacks if it is used alone in the lithium ion batteries. It has slow diffusivity rate, high volume change and low cycle ability, leading to cracking and delamination. This weakness is barely improved by using silicone nanowires facilitating the volume expansions.[19] To ameliorate the properties of silicone, it is suggested that the crystalline Si core can be replaced by carbon as it has less volume exchange.[20]

2.1 Recent progress in the graphene anode composites

Lithium ion batteries are comprised of three major components: a cathode, anode, and electrolyte (Fig. 2). The electrochemical reactions are the fundamental of the process when

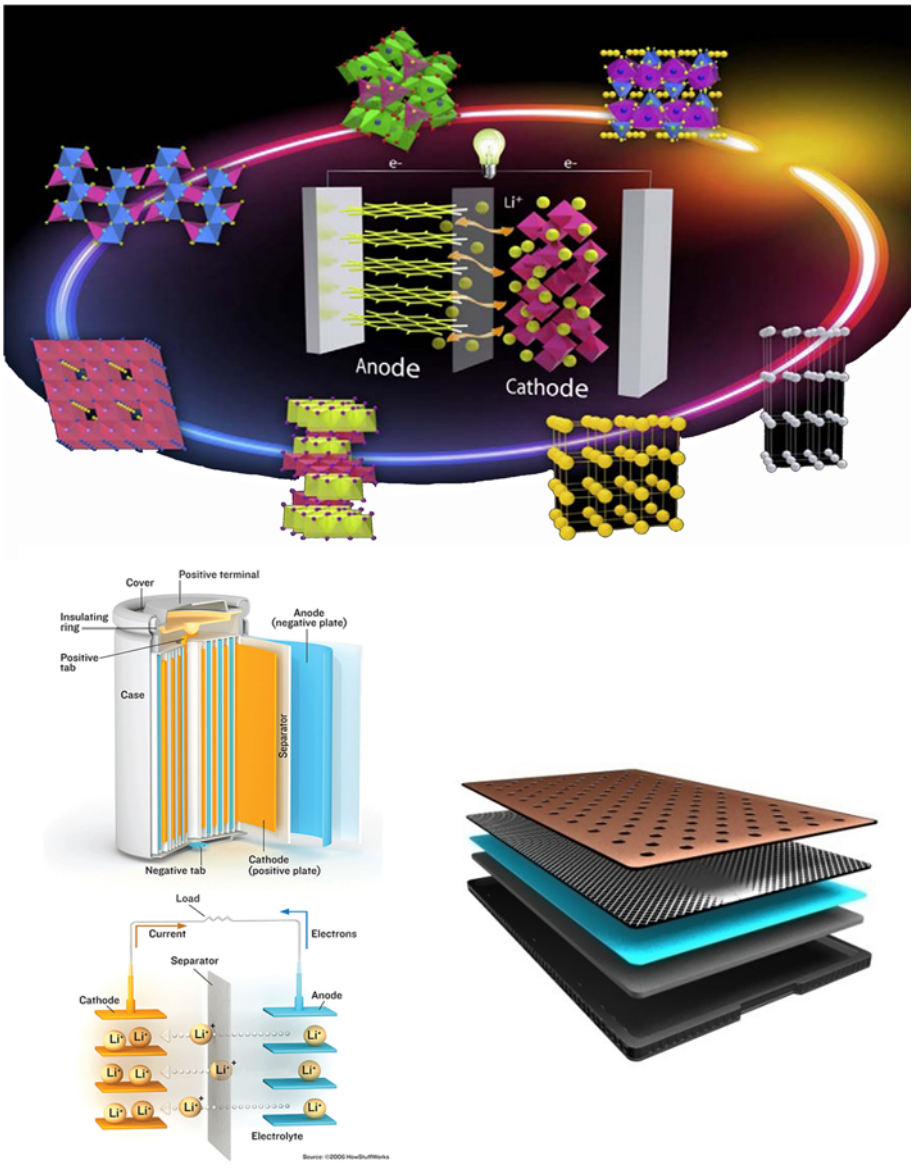

Fig. 2. Schematic of lithium-ion batteries.[21]

lithium ions travel from the cathode to the anode. Diffusion of lithium ion in the electrode materials can be occurred by a charge transfer process. This transfer by means of diffusional reaction is the case for determining the rate of lithium ion transportation. The progresses in the lithium ion technology can be categorized into the replacement of the carbonaceous materials with alternative low-voltage like lithium-accepting anode compounds with the aim of improving safety characteristics, the replacement of cobalt with nickel or manganese in the cathode structure with the aim of reducing cost and the environmental toxicity and the replacement of the liquid-like electrolyte with a polymer electrolyte (a plastic like membrane which can act both as an electrolyte and a separator) with the aim of optimizing battery design, reliability and flexibility.

Since the invention of first generation of the lithium-ion batteries, several carbonaceous anode materials are being used in the lithium-ion batteries.[22-24] In the earlier years, because of the limited rechargeability and safety hazard concerns of lithium-anode batteries carbonaceous anodes were considered as an appropriate case as the anodes. The cathode in cells having pure lithium anodes was used[25,26] and later pyrolytic carbon anode and metal oxide cathode (vanadium oxide and chromium oxide) were applied in the rechargeable batteries.[27] The low cost and low operational voltages of carbonaceous materials initially motivated

graphite and coke for the use of anodes (called soft anodes) in the lithium-ion batteries coupled with high voltage cathode like $LiCoO_2$, so that a battery operating in 4 V range largely commercialized.[28,29] Although recent years many alternative to carbonaceous anodes like lithium and metal alloys with much higher capacity have been reported, but they are prolonged to the so called pulverization effects which limits its practical use greatly. Therefore, carbonaceous materials remain in the center of the fabrication of anodes in lithium-ion batteries. The mechanism of lithium intercalation in soft carbon anodes is to develop through identified, reversible stages corresponding to progressive intercalation within separate graphene layers, reaching into the formation of LiC_6. The theoretical value of the discharge capacity of lithiated carbon is calculated to be 372 $mAh(gm)^{-1}$ based on the charge/discharge reaction 6C+Li p LiC_6,[30] extending the process to the range of few mV vs. Li. However, since this is below the decomposition limit of many of the common electrolytes, these anodes suffer from poor specific capacity and kinetics, although produces more safety and reversibilities.[31] Several forms of carbon with capacities higher than graphite and coke are being reported, including hard carbons. The charge storage mechanisms in these carbons are neither well understood nor is unique in all the forms of carbon anode.[32] Various kinds of carbon with wide range of crystallinity like carbon fibers and highly disordered forms of carbon (poly-p-phenylene (PPP)-based carbon) were studied as anode materials. Other forms of carbon studied are special types of low temperature forms of carbon, such as that derived from phenolic resin, mesocarbon microbeads (MCMB)-low temperature heat-treated MCMBs are reported with high capacities,[33] poly-p-phenylene (PPP)-PPP heat treated at 700°C in H_2 atmosphere has capacity of 680 $mAh(gm)^{-1}$.[34] Carbon and graphitic materials have large variety in microstructures, texture, morphology, and crystallinity, depending on their preparation processes and precursor materials, as well as of various forms such as powders, fibers and spherules.

A large number of various forms of composite materials of carbon and different other materials are being reported. For example, carbon-coated nanophase $CaMoO_4$, the nanocomposites of carbon nanotube with Sb and $SnSb_{0.5}$ tin-iron alloy, nanostructured SnO_2/C composite anodes, oxidized boron-doped carbon fiber, Si-C composite prepared by mechanical ball milling, carbon nanotube/nanohoneycomb diamond compositej, Si coated CNT, atmosphere carbon-coated tin anode, ordered mesoporous carbon, carbon-coated $CaWO_4$, rapidly solidified Ti-Si alloys/carbon composites, carbon coated Cu_6Sn_5 alloy-graphite composite, nano-porous Si/Graphite/C composite, silicon/disordered carbon nanocomposites, CoO-loaded graphitable carbon hollow spheres, carbon-coated $Si_{70}Sn_{30}$ nanoalloys, mesoporous carbon-tin nanocomposites, nano-sized cobalt oxide/mesoporous carbon sphere composites, coaxial MnO_2/carbon nanotube array electrodes, silicon-carbon composite, foam-like, microstructural SnO_2-carbon composite, Sn-Co-C composite anode, tin-carbon composite and silicon/graphite composites with TiN additive are the composite materials of carbon and different other materials are used for the coating of Li-ion batteries in the past decade.

Most of the charging and discharge capacity at anode (charging means lithium insertion into anode and discharging means lithium removal form carbon (opposite terminology as compared to the terminology for a cathode or the battery) are explained on the basis of cavity model (lithium ion not only intercalated into/out of the carbon layers but also doped in the nano cavities. For example, high capacity MCMBs has cavities with the size of 0.5 - 1.5 nm). However, graphene composites are recently considered as an attractive anode for the lithium batteries. The electronic structure of graphene follows from a simple nearest neighbor, tight-binding approximation. The graphene composite anode material offers improved cycle life which issues associated with graphite particle fragmentation and loss of capacity due to large expansion and contraction are eliminated due to the mechanically flexible graphene sheets that buffer volume expansion, enhanced electron transport which the highly conductive graphene provides a robust network with strong electrical continuity and high efficiency which the high surface area of graphene coated with a thin layer of ion-storage material ensures even distribution and interconnection of the ion storage material and the conductive graphene. Graphene has two atoms per unit cell results in two conical points per Brillouin zone where band crossing occurs, K and K'. Near these crossing points, the electron energy is linearly reliant on the wave vector (see Fig. 3).[35]

There are many structural models for the graphene/nanopartile anodes but six of them are more famous as they used for the experimentally approved functional nanocomposites (see Fig. 4). Graghene in its two dimensional form and with its unique structure can be a support for metal oxides with different size, shape and crystallinity. On the other hand, metal oxides can control the restacking of graphene as it acts as conductive pattern and facilitates the charge transfer.

There exist wet-chemistry techniques like in-situe deposition, sol-gel process and hydrothermal synthesis to prepare the graphene/nanoparticles. However, other methods such as milling can be applied to produce the grapghene/nanocomposite anodes. A scalable high-speed milling can be used to produce a nanocomposite made of SiC coated with few-layer graphene, with tin oxide nanoparticles trapped between the two. This material showed an exceptional high-reversible capacity for lithium-ion storage, reaching to almost two times higher than the theoretical capacity of the alloying reaction normally observed in common tin oxide anode materials.[36,37] Another nanostructure that can be produced

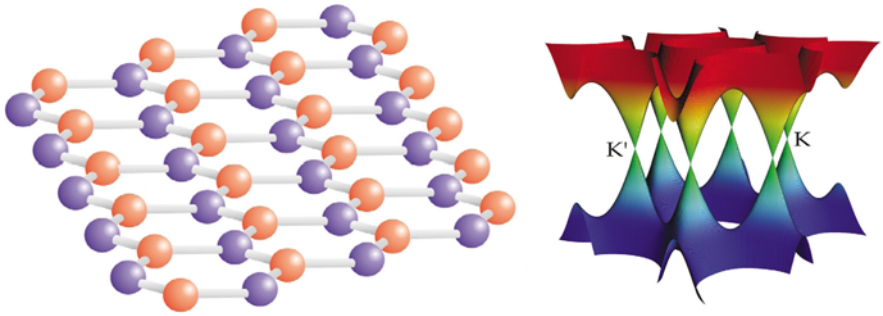

Fig. 3. Crystallographic and band structure of graphene. The conductance band contacts the valence at the *K* and *K'* points.[35]

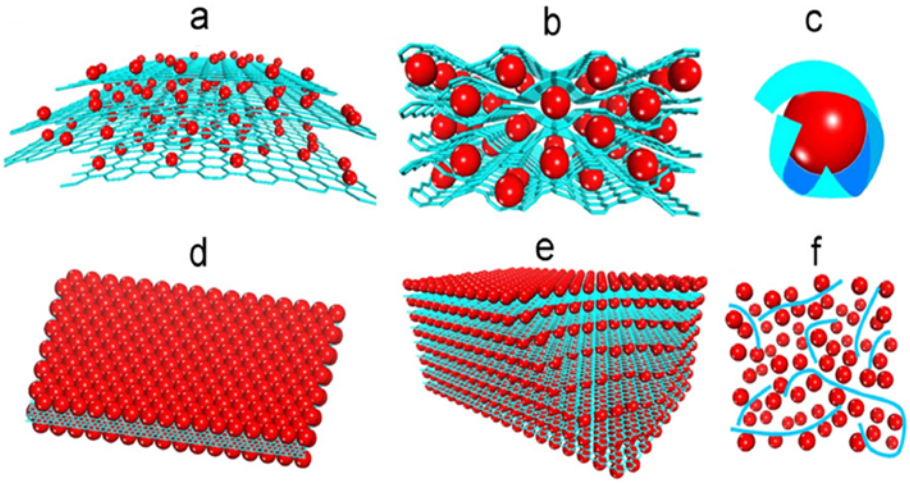

Fig. 4. Schematic of graphene/metal oxide composite's models: (a) anchored model, (b) wrapped model, (c) encapsulated model, sandwich-like model, (e) layered model, (f) mixed model. In the structures, red balls are metal oxide particles and blue scheme is graphene sheets.[3]

by the milling process is Bi/C and Bi/Al_2O_3/C nancomposites.[38] The interaction bismuth and alumina can be written as:

$$Bi_2O_3 + 2Al \rightarrow 2Bi + Al_2O_3. \quad (10)$$

The coulombic efficiency of the Bi/C nanocomposite was 71% at the first cycle. The irreversible capacity of the Bi/C nanocomposite was predicted to be 100 $mAhg^{-1}$. However, Bi/Al_2O_3/C nanocomposite showed better cycle retention with capacity of 400 $mAhg^{-1}$ after 10 cycles.

From another stand point, nanosize electrode materials can induce various effects on the reaction mechanism as well as the performance of lithium ion batteries, although the basic goal of using nanoscale dimensions is just to provide a short diffusion path.[39] As it is essential to enhance the energy density, the operating voltage should be increased. To do so both the cathode and anode materials should be selected in a way that the electrolyte and electrode (made of Sn, graphite and Si) have not burden a heavy discharge. The electrode materials expand because of the travel of lithium ions, inducing fatigue and as a result degrading by pulverization so the charge and discharge of the electrode can be controlled. Three dimensional porous and one dimensional nanowires have been used as the anode materials. Si-carbon core-shell nanowires, Si nanotubes and three dimensional porous Si particles have been characterized using butyl-capped Si solutions with ordered mesoporous silica, a porous anodized alumina membrane and spherical silica particles as templates.[40,41] It was shown that after cycling the morphologies were not significantly altered (see Fig. 5).

Metal oxides like CoO, Co_3O_4, CuO, NiO, and MnO showed a conversion reaction with lithium which is electrochemically reversible for hundreds of cycles.[42] The transition metal oxides have high specific capacities (700 $mAhg^{-1}$) but high polarization is demonstrated because of poor kinetics of conversion reactions, which is attributed to the high barrier energy to activate the breaking of the M-O bonds. In the binary alloy anode materials is also conversion reaction can be occurred because of some intermetallics like $CuGa_2$ and $NiGa_4$ forms nanosized inactive metallic grains and active Li-Ga grains.[43] This causes high polarization emanated from high activation energy to break the M-Ga and M-O bonds and make the overpotential of lthium reactions higher than delithiation reactions. A partial bonding between the

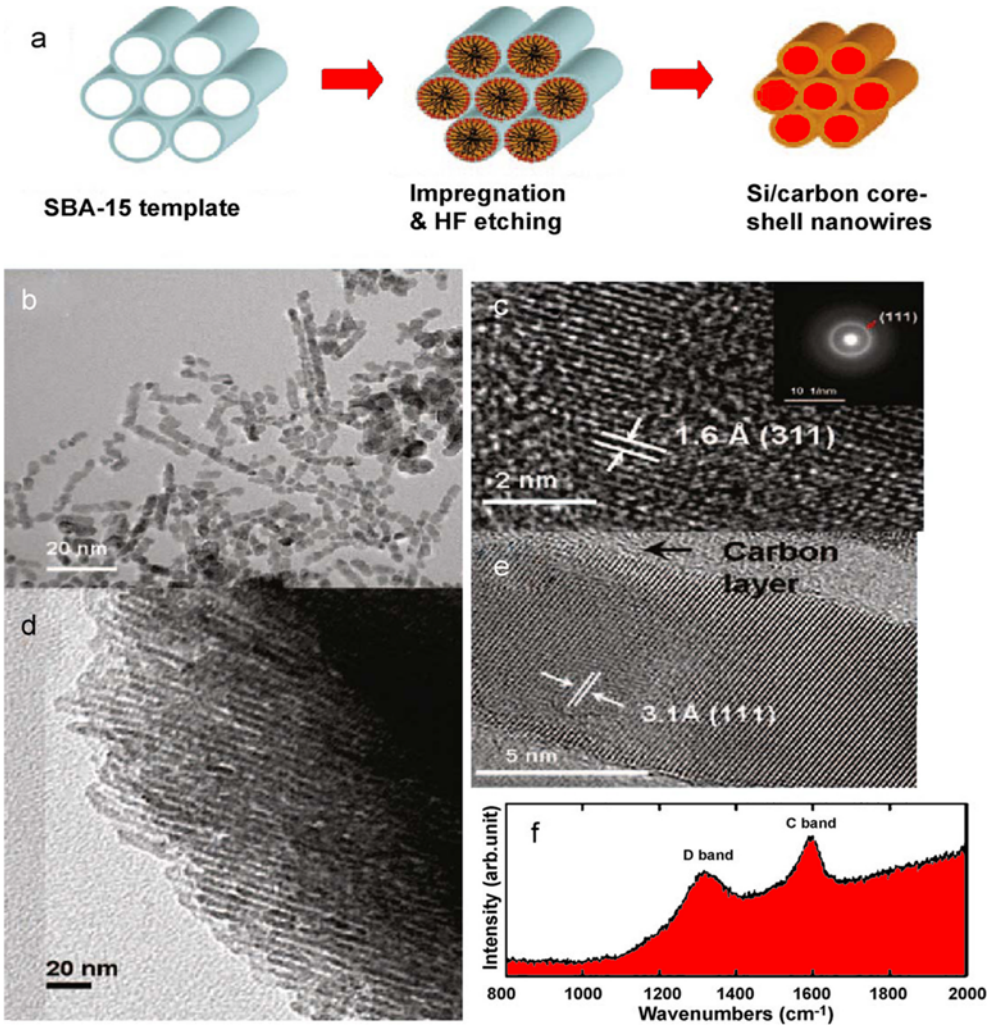

Fig. 5. (a) Schematic illustration of the preparation of Si-carbon core-shell nanowires. (b) TEM image of Si-carbon core-shell nanorods obtained from first impregnation. (c) Expanded TEM image of (b) (inset is the selected area diffraction pattern of (c)). (d) TEM image of Si-carbon coreshell nanowires obtained from fourth impregnation. (e) Expanded TEM image of (d) and (f) Raman spectrum of Si-carbon core-shell nanowires.[41]

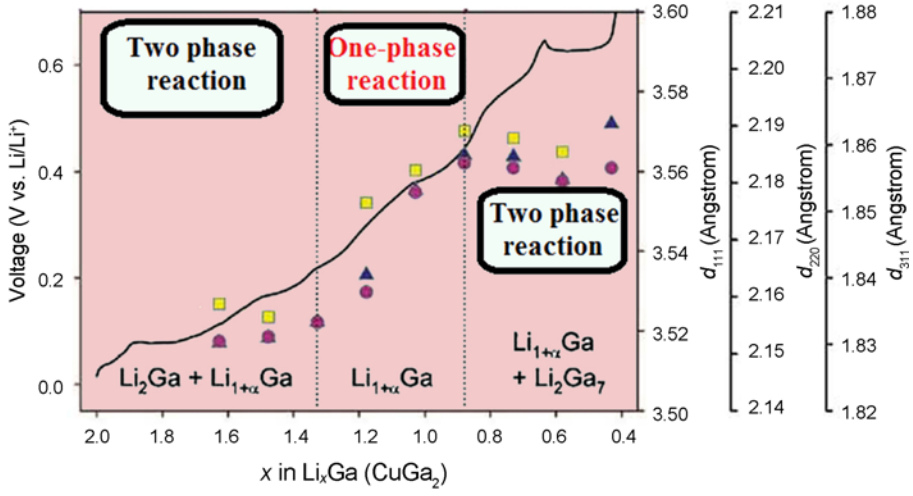

Fig. 6. *d*-spacing values of LiGa phase derived from the $CuGa_2$ electrode at 120°C.[46]

two nanograins is suggested using Raman and XRD analyses. While using nanocomposite Li_2Ga+M, a unique delithiation is observed, including the formation of Li-Ga phase (see Fig. 6). This behavior is also reported for In-Cu intermetallics,[44] MoO_2,[45] and (Cu, Fe, Co) GeO_3[46] materials.

Graphene has been used as an individual material for the lithium ion battery anodes, showed enhancement in storage and cycling.[47] This is associated with the higher surface area achieved in graphene.[48] This suggested that the graphene sheets for anode materials with discharge capacity of 560 $Ahgm^{-1}$ have better behavior. There are few reports to summarize possible ways for applying the carbon as the anode material.[49] Wu *et al.* reviewed the effect of mild oxidation of graphite, formation of composites with metals and metal oxides.[50] Microencapsulated graphite with nanosized silver and nickel metal particles to form composite anodes were developed and its study of suppression of cointercalation of solvated lithium ions into graphite is of great interest. It is proposed that nanomaterials, because of their reduced dimensions, can provide more improvement of intercalation/deintercalation rates, high charge/discharge and high power in the lithium ion batteries.[51] However, use of nanoparticulate graphite can form a reactive solid-electrolyte-interface layer on the graphite surface but on the other hand carbon nanosheets can produce more lithium storage capacity. Lithium diffusion along the edges of graphene together with chemical reduction prepared a armchair and zig-zag shape edge, made better charge/discharge rates and capacity.[50] It is important to note that the shape of the edge causes more increase in the Li^+ intercalation in comparison to single layer graphene.[52] It should be pointed out that the reactivity of carbons towards the electrolytes is greater than their reactivity at the basal planes because the carbon atoms at the edge planes of the graphene are not saturated in bonding valance, resulting in decomposition of the electrolyte solution during the charge process in the start cycle, lowering the coulombic efficiency η:

$$\eta = RD/EC \times 100 \quad (11)$$

where *RD* is the amount of lithium removed during discharge and *EC* is the amount of electrons consumed during charge. There are many ways to improve the efficiency in the begin cycles, including mild oxidation to decrease carbon atoms at the edge of graphene structure.[53] However, the defects as a result of chemical reduction can prepare electronic barriers to Li^+ repulsion effects. As the lithiation and delithiation reactions ($Sn^{+4.4}Li^+ + 4.4e^- \leftrightarrow Li_{4.4}Sn$) can be occurred by a large volume change, resulting in the pulverization of the particles and the electrical disconnection of the electrode, new anode materials are reported in many recent researches. For example, the anode part was improved using tin nanoparticles coated with carbon embedded in graphene (the size of the nanoparticles was about 50 - 200 nm).[54] To prepare the anode it was essential to use hydrothermal synthesis and subsequent annealing. It is reported that the reversible specific capacity of the nanocomposite is 662 $mAhg^{-1}$ at a specific current of 100 mAg^{-1} after 100 cycles, and 417 $mAhg^{-1}$ at the high current of 1000 mAg^{-1}. The graphene matrix not only can accommodate the volume change of Sn during charge-discharge but also facilitate the electron transport because of its high electronic conductivity. The nanoparticles can act as a barrier for the volume charge when coated on the carbon shells, giving the ability to avoid aggregation in the particles. One of the thing that is negatively affect the lithium batteries by this method is that the carbon shell is not elastic enough to balance the volume charge of thin so graphene nanosheets can be employed due to the especial character of graphene. Figure 7 shows a comparison between the SnO_2/graphene and SnC/graphene.

Although SnO_2 has high theoretical storage capacity (782 $mAhg^{-1}$) based on an alloying mechanism, $Sn + xLi^+ + xe^- \leftrightarrow Li_xSn$ (where x can be between 0 and 4.4), its application in practical lithium-ion batteries is limited by the poor cycling performance arising from the huge volume changes of about 300% during Li^+ insertion/extraction process, leading to mechanical failure and the loss of electrical contact of the anode.[55] Reduced graphene oxide/SnO_2 oxide composite can be prepared by homogenous coprecipitation, showing 2140 $mAhg^{-1}$ and 1080 $mAhg^{-1}$ capacities for the first discharge and charge, respectively.[56] Cycling performance of the composite was shown capacity is about 649 $mAhg^{-1}$ at the 30th discharge. In this technique, the precipitated $SnCl_4$ was homogenized in a suspension of graphene oxide platelets using urea and subsequent reduction of the graphene oxide was performed with hydrazine under microwave irradiation to decorate the graphene oxide plates with SnO_2 nanoparticles and at the end annealing of the slurry was conducted at 500°C for 3 h under a nitrogen atmosphere. During the hydrolysis, urea released hydroxyl ions slowly in the suspension, leading to the formation of $Sn(OH)_4$.

$$CO(NH_2)_2 + 3H_2O \rightarrow 2NH_4^+ + CO_2 + 2OH^-. \quad (12)$$

$$Sn^{4+} + 4OH^- \rightarrow Sn(OH)_4. \quad (13)$$

$$Sn(OH)_4 \rightarrow SnO_2 + 2H_2O. \quad (14)$$

The SnO_2/graphene composite can also be synthesized by a simple hydrothermal method for high-capacity lithium storage. A flower-like SnO_2 nanorod clusters with the size of 800 nm are the result of the synthesize process (Fig. 8). The flower-like SnO_2/graphene composite displayed acceptable results in the first discharge and charge by reaching the capacity to 1588 and 1240 $mAhg^{-1}$ at the current density of 50 mAg^{-1}, respectively.[57] After 40 cycles at different current densities of 50, 100, and 500 mAg^{-1}, the reversible discharge capacity was maintained at 730 $mAhg^{-1}$.

However, the electrochemical performance of SnO_2-based nanocomposites can be improved by the combination of the

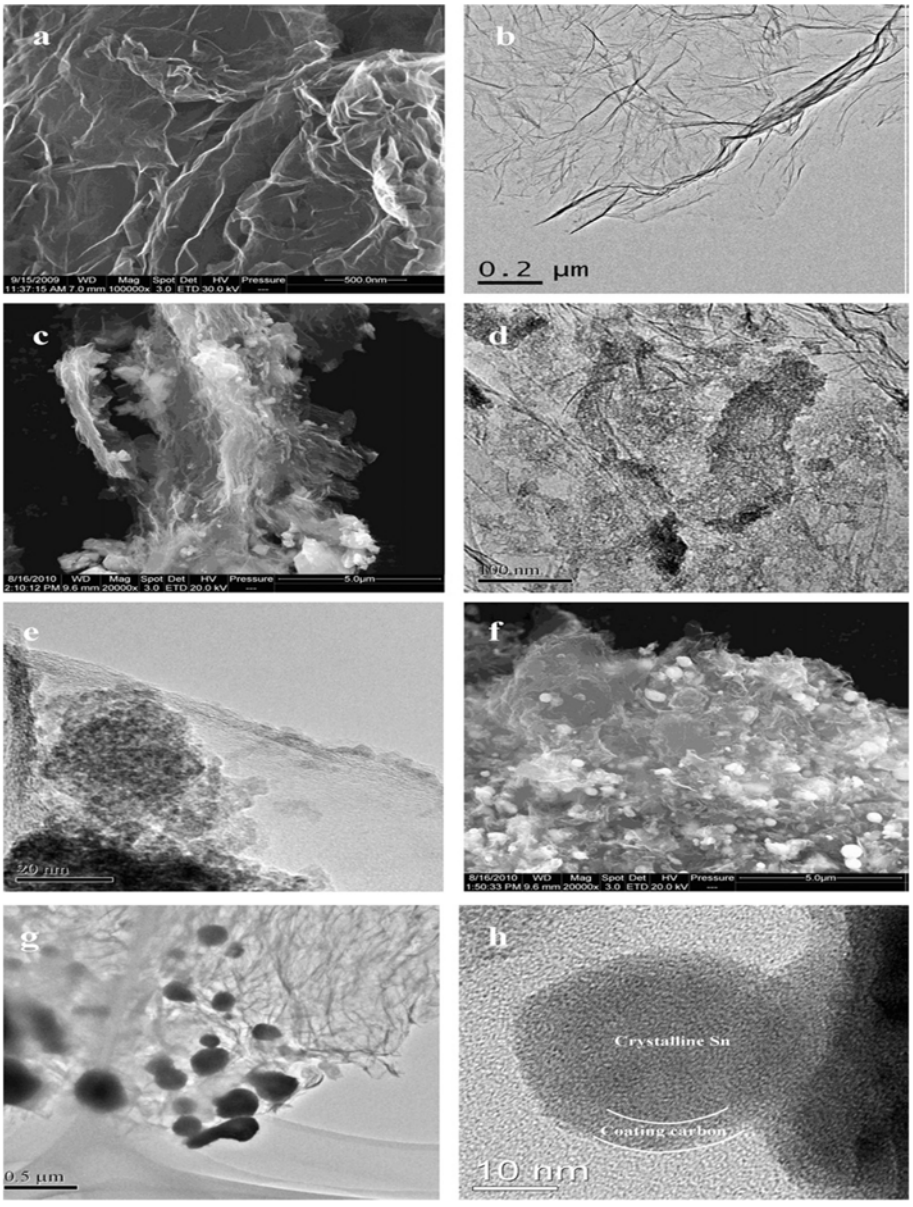

Fig. 7. SEM and TEM images of (a,b) graphene, (c-,f) SnO_2/graphene and (g,h) SnC/graphene.[54]

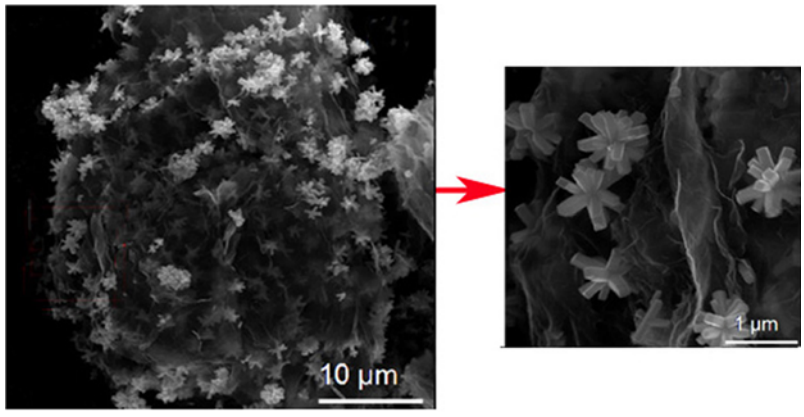

Fig. 8. SEM image of flower-like SnO_2-graphene in different magnifications.[57]

nanocomposite with other oxides, such as Li_2O-CuO-SnO_2,[58] RuO_2-SnO_2,[59] $CuFe_2O_4$-SnO_2,[60] SiO_2-SnO_y,[61] CuO-SnO_2,[62] In_2O_3-SnO_2[63] and NiO-SnO_2-C.[64] As the development of the anodes are aimed to make them more efficient, the combination of the nanoparticles is also shown to be a fine idea in order to have better lithium ion batteries. For instance, Fe_3O_4-SnO_2-graphene ternary nanocomposite can be synthesized using a gas-liquid interfacial synthesis process. This combination exhibited a high reversible specific capacity of 1198 $mAhg^{-1}$ in 115th cycle at a specific current of 100 mAg^{-1}. This performance can be associated with the synergistic effect of graphene and metal oxides and both Fe_3O_4 and SnO_2.[65] It was noticed that at a high specific current of 2000 mAg^{-1}, the reversible capacity remained as high as 521 $mAhg^{-1}$. It was revealed that the Fe_3O_4-SnO_2 nanocomposite prepared by the gas-liquid interfacial reaction can be aggregated into large particles. The large particles could be easily pulverized due to the asymmetrical volume change during Li^+ insertion/extraction process, resulting in capacity decay as an anode material for lithium-ion batteries. As it is shown in Fig. 9. the graphene sheets are distributed between the Fe_3O_4-SnO_2 nanoparticles and the porous composite with

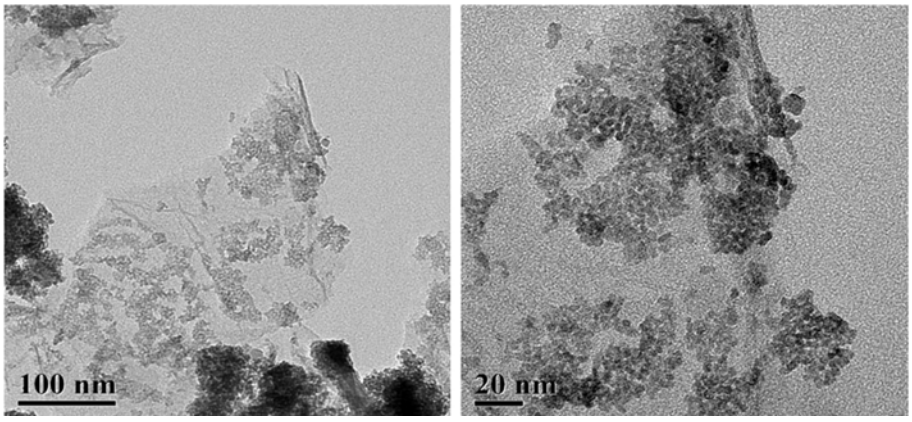

Fig. 9. TEM images of Fe_3O_4-SnO_2-graphene nanocomposite in different magnifications.[65]

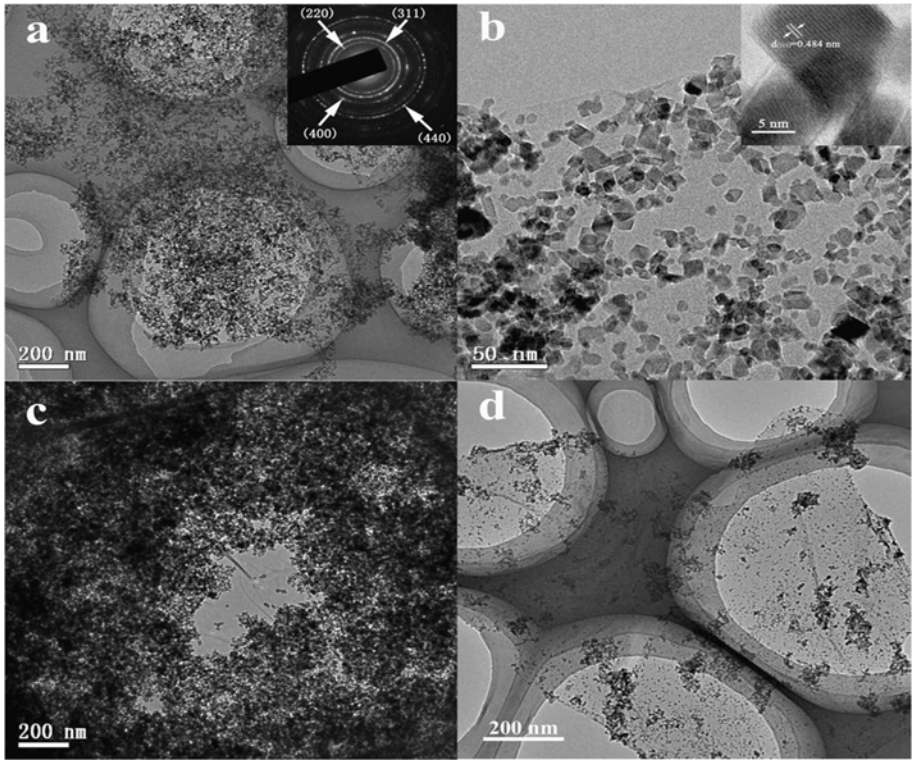

Fig. 10. Transition electron microscopy images of Fe_3O_4/graphene nanocomposites. (a and b) Fe_3O_4/graphene (50 wt. %), (c) Fe_3O_4/graphene (95 wt. %) and (d) Fe_3O_4/graphene (42 wt. %).[68]

large amount of void spaces was formed which gives good cycle performance and can perform as a buffer for large volume changes of the nanoparticles during lithium ions insertion/extraction process.[66] Carbon-coated SnO_2 nanoparticle/graphene nanosheets is also an interesting idea as it shows fine electrochemical performance with high capacity of 757 $mAhg^{-1}$ after 150 cycles at 200 mAg^{-1}.[67]

Transition metal oxides, such as Fe_3O_4 and CuO are known as potential alternative anode materials. In another research, a composite of Fe_3O_4 nanoparticles and graphene nanosheets was prepared using a single step method.[68] To prepare the graphine composite, ethylene glycol mixed with Fe^{3+} species to form Fe_3O_4 is applied and the reduction of graphene oxide into graphene, and the preferential attachment of fine Fe_3O_4 nanoparticles onto graphene sheets are performed in one step. The method and prepared composite (18.5 wt. % graphene) showed high reversible capacity, reaching to a capacity of 750 $mAhg^{-1}$ after 40 cycles at 50 mAg^{-1}. As it is shown in Fig. 10, TEM image of Fe_3O_4/graphene (50 wt. %) showed that the Fe_3O_4 nanoparticles are homogeneously distributed on the basal plane of graphene nanosheets. A ring-like pattern is appeared indicating Fe_3O_4 nanoparticles are polycrystalline. Cyclic voltammograms showed that during the cathodic polarization process of the Fe_3O_4-SnO_2-graphene nanocomposite some unique peaks can be observed at different voltages. The peaks are directly related to the formation of the solid-electrolyte interface layer on the surface of the active material, reduction of SnO_2 into Sn and the synchronous formation of Li_2O.[69-72] The vicissitudes of the voltammograms can be stated by the following reactions.

$$SnO_2 + 4Li^+ + 4e^- \rightarrow 2Li_2O + Sn. \quad (15)$$
$$Fe_3O4 + 8Li^+ + 8e^- \rightarrow 3Fe + 4Li_2O. \quad (16)$$
$$Sn + xLi^+ + xe^- \rightarrow Li_xSn\ (0 \le x \le 4.4). \quad (17)$$
$$2C + Li^+ + e^- \rightarrow LiC_2. \quad (18)$$
$$SnO_2 + 4Li^+ + 4e^- \rightarrow 2Li_2O + Sn. \quad (19)$$
$$Fe_3O_4 + 8Li^+ + 8e^- \leftrightarrow 3Fe + 4Li_2O. \quad (20)$$
$$Sn + xLi^+ + xe^- \leftrightarrow Li_xSn\ (0 \le x \le 4.4). \quad (21)$$
$$2C + Li^+ + e^- \leftrightarrow LiC_2. \quad (22)$$

It is interesting to note that the reduction of Fe_3O_4 led to the formation of Fe nanograins dispersed in a lithia matrix (Li_2O). The first reversible specific capacity of the Fe_3O_4-SnO_2 nanocomposite is as high as 667 $mAhg^{-1}$. However, the reversible specific capacity quickly fades and only 253 $mAhg^{-1}$ remains in the 50th cycle, showing poor cycling performance. In contrast, the reversible specific capacity of Fe3O4-SnO_2-graphene nanocomposite is constantly above 900 $mAhg^{-1}$ during the fifty cycles, exhibiting significantly enhanced cycling stability. The improved cycling performance of the Fe_3O_4-SnO_2-graphene nanocomposite can be attributed to the performance of the ultrathin graphene sheets as they can not only act as a barrier to prevent the aggregation of Fe_3O_4-SnO_2 nanoparticles, but also suppress the aggregation of the in situ formed nanoparticles like Fe, Sn and Li_2O during discharge/charge process[73] and the porous graphene sheets can provide a void space, which help to accommodate the volume changes of Fe_3O_4-SnO_2 nanoparticles during Li^+ insertion/extraction process.[74]

In another work, SnO_2 nanorods were grown on graphite by a simple hydrothermal method. The nanocomposite showed a current density of 50 mA g^{-1} in a voltage range from 0 to 3.0 V at first, second and tenth cycles.[75] The nanocomposite illustrated a lithium insertion capacity of 1197 $mAhg^{-1}$ and a reversible charging capacity of 872 $mAhg^{-1}$ with coulombic efficiency of 73%. Reversible capacity of 627 and 408 $mAhg^{-1}$ was achieved after 10 and 40 cycles, respectively. It should be noted that SnO_2 nanorods were grown based on the following reactions (see Fig. 11).

$$Sn^{4+} + OH^- \rightarrow Sn(OH)_4. \quad (23)$$
$$Sn(OH)_4 + 2OH^- \rightarrow [Sn(OH)^6]^{2-}. \quad (24)$$
$$[Sn(OH)_6]^{2-} \rightarrow SnO_2(\text{nanoroads}) + 2H_2O + 2OH^-. \quad (25)$$

Other metallic elements like Zn,[76] Ag,[77] and aluminum[78,79] can cover the surface of graphite. Ag increases the conductivity of the lithium storage sites, reversible capacity, rate capability and cycling behavior[80,81] and Al decreases charge-transfer resistance and as a result enhances the cycling behavior.[82]

Nitrogen-doped graphene nanosheet is another anode that showed an increase in the capacity with charge/discharge

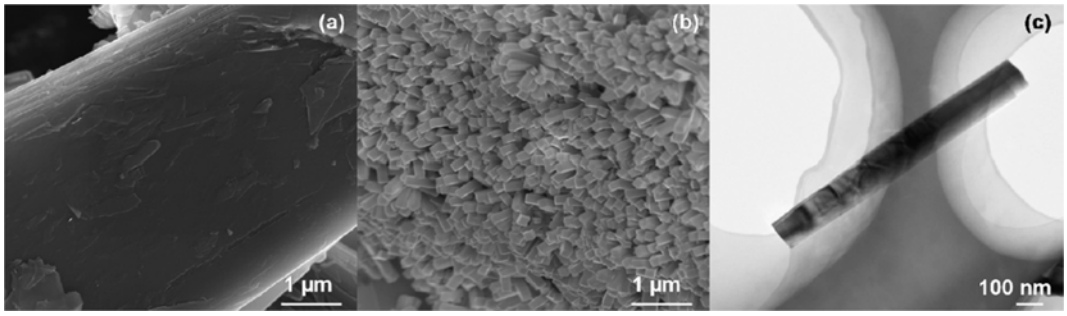

Fig. 11. (a) SEM pattern of graphite, (b) SEM pattern of SnO_2/graphite composite, (c) TEM pattern of single SnO_2 nanorod.[75]

cycles.[83] This anode showed a specific capacity of 684 $mAhg^{-1}$ in 500 cycle and 452 $mAhg^{-1}$ in 100 cycle. It is believed that the reactivity of the grapheme sheets with lithium ion is different along the plane and also along the zigzag and armchair edges.[84] Since the lithium ion adsorption is always along the two sides/planes and the edges, it is expected the anode shows higher capacity. In view of the fact that the grapheme powders are disordered the sheets are randomly oriented making it isotropic in all the directions so storage of the lithium ions is isotropic causing an increase in the capacity of the anode. The disordered graphene-based anodes can prevent any kinds of pulverization effect improving the stability of the anodes while discharging with different current densities. It should be noted that reactivity of the lithium ions towards grapheme oxides or grapheme-metal composites is higher than towards pure graphene. Sol-gel method has shown to be an appropriate technique to prepare $Li_4Ti_5O_{12}$/graphene composite.[85] The $Li_4Ti_5O_{12}$-graphene composite presented a higher capacity than $Li_4Ti_5O_{12}$ at high current rate. It was shown that when the $Li_4Ti_5O_{12}$/graphene composite discharged to 0 V capacity of about 430 $mAhg^{-1}$ can be achieved. In a thermodynamic and structural study, properties of Li_xTiO_2 spinel were investigated by pseudopotential ground state energy calculations in generalized gradient approximation at 300 K, using Monte Carlo simulation.[86] It was determined that there is a two-phase region for $Li_{(0.5-1)}TiO_2$ which the phases are different in the regions of reach lithium in $Li_{0.5}TiO_2$ and $LiTiO_2$ in which lithium occupied the crystallographic 8a and 16c sites of the phases, respectively.

The other promising nanocomposite is CeO_2-graphene which can be easily prepared by hydrothermal method.[87]

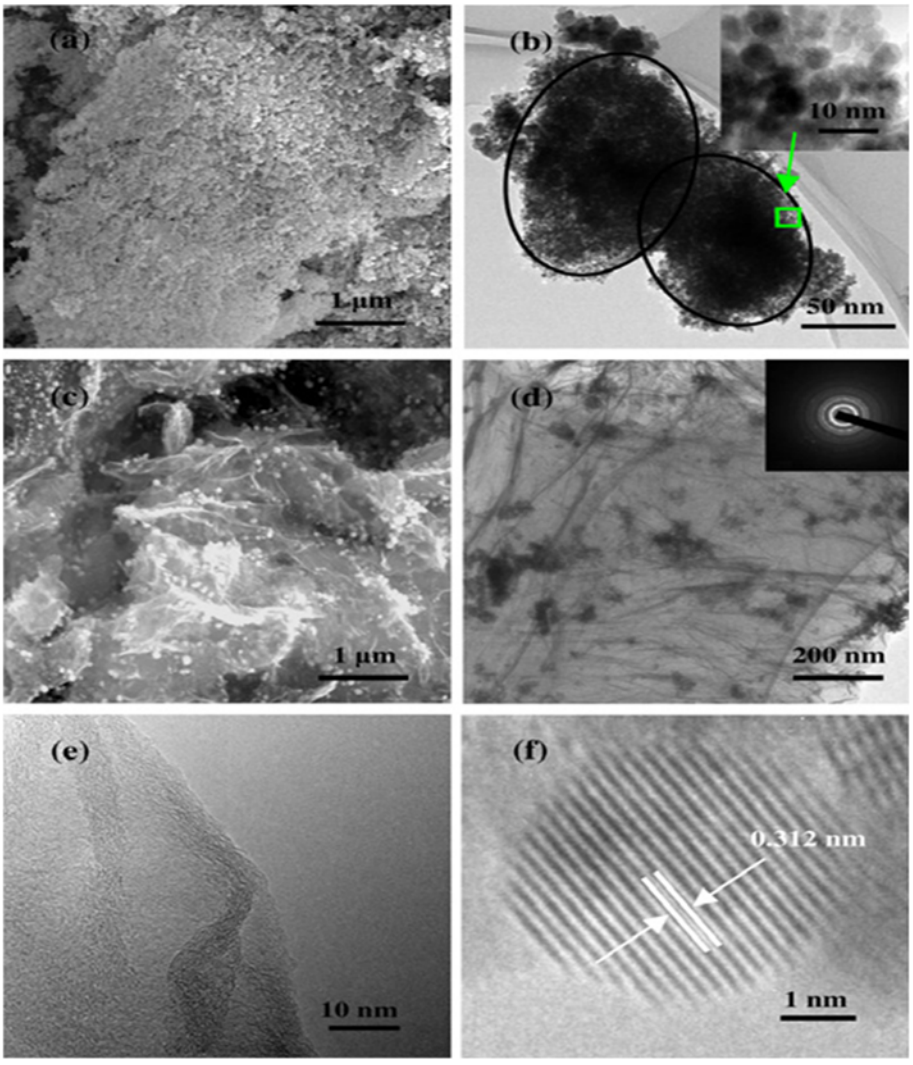

Fig. 12. (a) SEM image of CeO_2, (b) TEM image of CeO_2, (c) SEM image of the CeO_2-graphene nanocomposite, (d) TEM image of the CeO_2-graphene nanocomposite, (e) TEM image of graphene nanosheets in the nanocomposite, and (f) high resolution TEM image of a single particle of CeO_2 in the nanocomposite.[87]

Microstructural development of the nanocomposite showed quasi-spherical CeO_2 particles with a size of 100 nm were dispersed randomly on the graphene matrix (Fig. 12).

The CeO_2-graphene electrode showed high discharge and charge capacities in the first cycle, of about 1469 and 991 $mAhg^{-1}$, respectively. However, after 100 cycles the nanocomposite displayed relatively low capacity of 605 $mAhg^{-1}$. The advantage of using CeO_2-graphene is that the CeO_2 quasi-spherical particles can be homogeneously dispersed across the surface of the graphene nanosheets, preventing the CeO_2 particles from agglomerating. Thus, the volume change of CeO_2 during the charge-discharge process can be effectively occurred. A facile process for preparing SnS_2/graphene hybrid was developed by solution phase method employing L-cysteine as a complexing, sulfide source and reducing agent. It was demonstrated that the SnS_2 layer with some defects supports the graphene surface. The few-layered SnS_2/graghene exhibited capacity of up to 920 mAh g^{-1} with fine cycling stability and high-rate capability.[88] As the SnS_2 has some morphological similarities to graphene, it can be another promising composition in future of the anodes in the lithium ion batteries. The delocalized π-conjugation system of graphene can interact with the outer electrons of the S atoms in the SnS_2 nanosheets to support fast charge transfer in the electrode reaction. In this technique, L-Cysteine was dissolved in deionized water and $SnCl_4 \cdot 5H_2O$ was added. So, Sn^{4+} ions were easily complexed with L-Cysteine. The solution and the as-prepared graphene oxide were fully mixed under hydrothermal conditions at 180°C for 12 h to form a uniform distribution of the layered SnS_2 on graphene sheets (see Fig. 13).

The electrochemical test showed that in the potential range of 0.01 - 0.5 V, lithium ions alloyed with the Sn metal and form a series of Li_xSn_Y alloys. For the subsequent cycles, charge and discharge sharp areas were detected in the 0.5 - 0.7 V and 0.5 - 0.01 V vs. Li+/Li potential regions. However, it can be indicated that Li_2S, LiC_6, Li and Li_xSn were observed. It was shown that the capacities from the first discharge and charge (delithiation) cycles were 1309 and 462 mAh g^{-1} for the layered SnS_2 electrode, and 1664 and 705 $mAhg^{-1}$ for the layered SnS_2/graphene hybrid electrode. It is also demonstrated that with ten times increase in current density to 1000 mAg^{-1}, the specific capacity was as high as 600 $mAhg^{-1}$. TiO_2 graphene is another nanocomposite that can be synthesized by a facile gas/liquid interface reaction.[89] The electrochemical performance showed specific charge capacity of 499 mAh g^{-1} can be obtained at a current density of 100 mAg^{-1}. The TiO_2-graphene nanocomposite exhibited specific charge capacity of 150 $mAhg^{-1}$ at a high current density of 3000 mAg^{-1}. The advantage of this nanocomposite is that the oxygen-containing groups on the graphene sheets can be reduced after the heat treatment and residual functional groups including the OH and COOH on the surfaces of graphene sheets can interact strongly with the metal ions during the synthesis process (see Fig. 14). The random hybridization of TiO_2 nanoparticles and ultrathin graphene sheets formed a three-dimensional porous structure of the TiO_2-graphene nanocomposite. The small nanoparticles provided short path lengths for electron and lithium-ion transport during the lithium ion insertion/extraction process, resulting in excellent rate capability.

It has been reported that when graphene was added to artificial graphite as a conductive material, the lithium ion battery showed higher reversible capacity and better cycling stability.[90] It has been also stated that MO/graphene composites increased the reversible capacities compared to carbonaceous materials because of the formation of the conductive graphene network with nanosized MO particles and

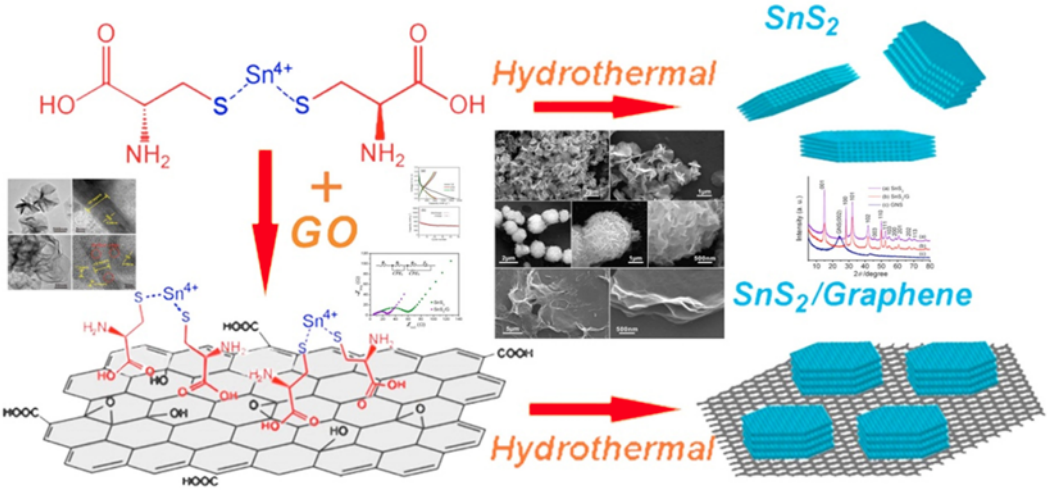

Fig. 13. Schematic of the layered SnS_2 and SnS_2/graphene by a solution-phased method and SEM images of the layered SnS_2 prepared by hydrothermal route and synthesized by facial process.

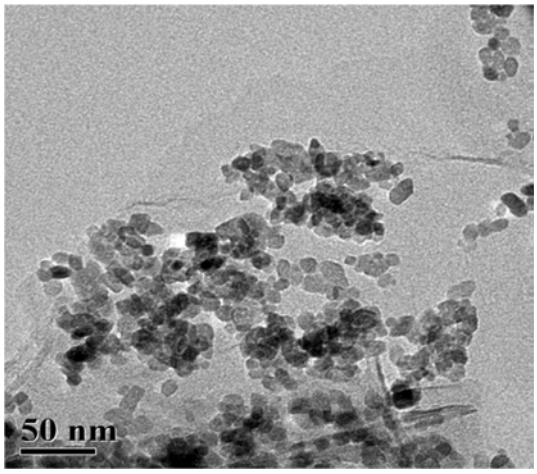

Fig. 14. TEM observation of the TiO_2-graphene nanocomposite.[89]

the elastic buffer by graphene.[91] When graphene sheets were applied the aggregation of the TiO_2 nanoparticles was prevented and electrochemical reactive activity was increased. As a result, the specific charge capacity of the TiO_2 in TiO_2-graphene nanocomposite was dramatically enhanced. The interesting thing was the estimation of the specific charge capacity of the TiO_2 in TiO_2-graphene by a linear equation (Eq. (26)).

$$C_T = (C_{TG} - \omega C_G) / (1 - \omega) \quad (26)$$

where C_T, C_{TG}, and C_G are defined to be the specific charge capacities of the TiO_2 in TiO_2-graphene nanocomposite, TiO_2-graphene nanocomposite, and graphene sheets, respectively. It is reported that the specific charge capacity of the composite is 150 $mAhg^{-1}$ at a current density of 3000 mAg^{-1} between 0.01 and 3.0 V, the Warburg impedance coefficient (σ_w) is 81.17 $\Omega\ cm^2\ s^{-0.5}$ and the values of the uncompensated bulk resistance (R_Ω) and charge-transfer resistance (R_{ct}) are 0.82 and 36.34 Ω, respectively. As the use of nanocomposites in the form of oxide combination is of great interest, NiO-graphene are introduced and synthesized by a liquid phase deposition method. The NiO-graphene demonstrate a capacity of 646.1 mAh g^{-1} after 35 cycles at a current density of 100 mAg^{-1}. At the current density of 400 and 800 mAg^{-1}, the oxide-graphene showed capacity of 509 and 368.5 mAh g^{-1}, respectively.[91] MnO nanocrystals were supported the graphene in the anode materials of lithium ion batteries by a simple chemical-wet impregnation followed by the thermal reduction route. The MnO-graphene anode demonstrated a reversible capacity of 635 $mAhg^{-1}$ at 0.2 C in the voltage range between 0.01 and 3.5 V.[92] On the other hand, Si/graphene oxide nanocomposite films prepared by thermal reduction of Si/graphene oxide nanocomposite, using an aqueous suspension of graphene oxide nanosheets, was claimed to have a capacity of 1921 $mAhg^{-1}$ and 524 $mAhg^{-1}$ for the first charge-discharge cycle with reversible capacity of 27%.[93] After 30 cycles, the capacity retention ratio of the composite film was about 977 $mAhg^{-1}$ and suitable cyclic performance was confirmed by relatively stable capacity of 786 $mAhg^{-1}$ at a current density of 50 mAg^{-1} after 300 cycles.

It is believed that the initial coulombic efficiency, discharge specific capacity and cyclic stability of the film were better than Si/graphene composite produced by reduction of Si-graphene oxide using hydrazine monohydrate because of homogeneous distribution of Si nanoparticles among the graphene oxide sheets. The homogenous structure prevented the aggregation of Si nanoparticles and made elastic matrix to accommodate the mechanical stresses/strains of Si phase. However, oxygen functionalities like -O- and -OH- left attached to carbon because of the relatively mild reduction condition and interaction with the surface of the Si nanoparticles.[94] Graphene/nanosized silicon composites were also prepared, by two methods, one in aqueous solution and then annealed at 500°C and in the second method, the graphene sample was prepared by fast heat treatment of expandable graphite at 1050°C and then blend the solution mechanically. In both cases, homogeneous composites were formed and the presence of graphene in the composites has been proved to effectively enhance the cycling stability of silicon anode in the lithium-ion batteries. The specific capacity of the composite was as high as 2753 $mAhg^{-1}$, which was attributed to the role of nonosheets as a buffer on the volume change produced by large amount of void spaces.[95,96] At a current density of 400 mA/g (rate of 0.5C), the charge capacity of the composite stayed 590 $mAhg^{-1}$ up to 50 cycles. When increasing the current density to 1000 mAg^{-1} (rate of 1.3C), the composite delivered a capacity of 270 $mAhg^{-1}$ up to 50 cycles.[96]

CuO and Co_3O_4/reduced graphene oxide was synthesized by N-methyl-2-pyrrolidone solvent[97] and a simple in situ reduction process[98] and it was shown that the metal oxides caused an increase in the initial Coulombic efficiency and decreased the number of functional groups, leading to irreversible lithium ion intercalation on the surface of the graphene layers. Co_3O_4-graphene nanocomposites can also be synthesized by solvothermal method. After using this technique, electrochemical tests revealed that the Co_3O_4-graphene nanocomposite improved cycling stability and demonstrated high reversible lithium storage capacity and superior rate capability reaching to capacity of 1310 $mAhg^{-1}$ and 1090 $mAhg^{-1}$ for 40 cycles at a current density of 100 mAg^{-1} and 1000 mAg^{-1}, respectively.[99] In the simple in situe reduction process, the Co_3O_4/graphene anode exhibited a capacity of 800 $mAhg^{-1}$ reversibly at a 200 mAg^{-1} rate in the voltage range between 3.0 and 0.001 V. At a current rate as high as 1000 mAg^{-1}, the Co_3O_4/graphene anode showed 550 $mAhg^{-1}$.[100] Co_3O_4 nanoparticles can have 1-D structure

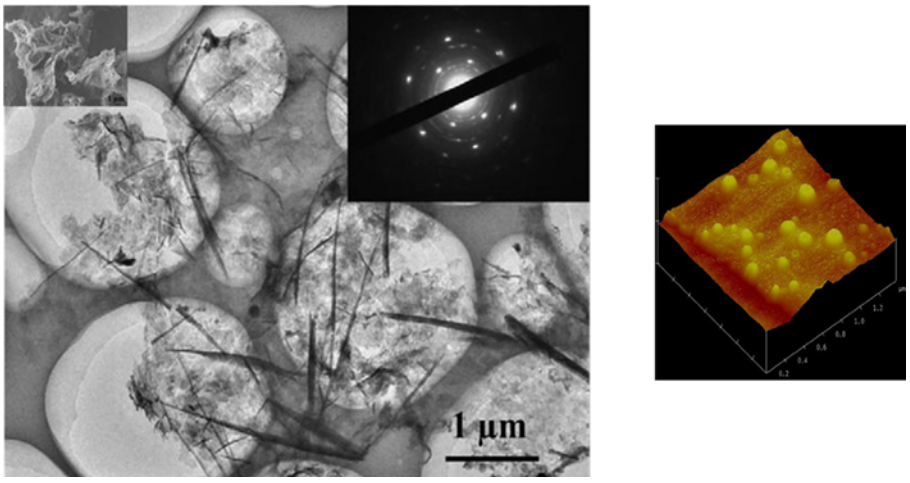

Fig. 15. TEM image of Co_3O_4-graphene nanocomposites.[99]

with higher aspect ratio, causing higher aggregation into larger particles during discharge/charge process and limiting the transportation of ions and electrons (see Fig. 15). As it can be seen, the rod-like Co_3O_4 with 30 nm in diameter and 2 μm in length is attached to the sheet-like graghene structure. The reversible capacity of Co_3O_4-graphene nanocomposite was increased with the increase of cycling numbers, reaching to 1300 $mAhg^{-1}$ after 40 cycles, which was attributed to the gradual activation of nanocomposites in the first cycles.

The Co_3O_4-graphene nanocomposite kept a reversible capacity of 1104, 1189, 1128 and 1090 mAh g^{-1} at the current density of 100, 200, 500 and 1000 mAg^{-1}, respectively. The Co_3O_4-graghene nanocomposites during the cycling process can have the following reaction:

$$CoO_4 + 8e^- + 8Li^+ \leftrightarrow 3Co^0 + 4Li_2O. \quad (27)$$

MoO_2/Graphene composite synthesized by a one pot in-situ low temperature solution phase reduction method, showed relatively high capacity of 770 $mAhg^{-1}$, and cycling stability of 550 mAh g^{-1} at a current density of 540 mAg^{-1}.[101] On the other hand, Si nanoparticles are reported to be dispersed between graphene sheets and supported by a three dimensional network of graphite formed by reconstituting regions of graphene stacks. This composition demonstrated a storage capacity of 2200 $mAhg^{-1}$ after 50 cycles and 1500 $mAhg^{-1}$ after 200 cycles.[102] However, in another work the Si nanoparticles were prepared by a different route using freeze-drying process and thermal reduction,[103] which showed a significant improvement in the properties of the anodes. The Si nanoparticles were also encapsulated in a graphene nanosheet matrix by in-situ filtration method. The electrochemical results showed that graphene-Si composite film has discharge capacity of 708 $mAhg^{-1}$ in 100 cycles. The graphene-Si nanocomposite gave a reversible capacity of 708 $mAhg^{-1}$ without obvious capacity loss over 100 cycles.[104] Copper oxide hollow nanoparticles/graphene-nanosheet composites are another type of the anode materials which can be prepared by the Kirkendall-effect approach. The reversible capacity of the composite was reported to be 640 $mAhg^{-1}$ at 50 mAg^{-1}. The reversible capacity reached to 485 $mAhg^{-1}$ at 1 Ag^{-1} and remained at 281 $mAhg^{-1}$ after 500 cycles. NiSb/graphene and $FeSb_2$/graphene nanocomposites can be considered as the other kind of nanocomposites and they can be fabricated by a facile one-step solvothermal route.[105] The NiSb/praphene nanocomposite showed capacity of 855 $mAhg^{-1}$ at the first charge and of 414 mAh g^{-1} at the first discharge. After 30 cycles, a capacity close to 280 $mAhg^{-1}$ was maintained for NiSb/graphene. The enhanced cycling stability is attributed to the buffering effect of graphene that improved the large volume changes and the confinement effect of graphene that restrains the aggregation of the NiSb nanoparticles. In recent years, $LiFePO_4$ has been widely studied as the cathode active material for lithium-ion batteries because of low-cost, low toxicity and relatively high theoretical specific capacity of 170 $mAhg^{-1}$[106] but the idea of having $LiFePO_4$/graphene might be cool as it can improve the performance of anode materials.[107] The $LiFePO_4$/graphene composites exhibited capacity of 160.3 $mAhg^{-1}$. The polarization between the charge and discharge plateaus was also reduced from 82 mV to 39 mV. The highly stable reversible capacity of 81.5 $mAhg^{-1}$ was obtained at the highest current densities of 10 C (see Fig. 16). In contrast, graphene/Co_3O_4 composite kept reversible capacity of 800 $mAhg^{-1}$ at 50 mAg^{-1}. The reversible capacity of the Co_3O_4/graphene composite and Co_3O_4 at other rates is 715 and 239 $mAhg^{-1}$ at 150 mAg^{-1}, 631 and 122 $mAhg^{-1}$ at 250 mAg^{-1}, and 484 and 53 $mAhg^{-1}$ at 500 mAg^{-1}, respectively.[108]

Aqueous suspensions of delaminated NiMn layered dou-

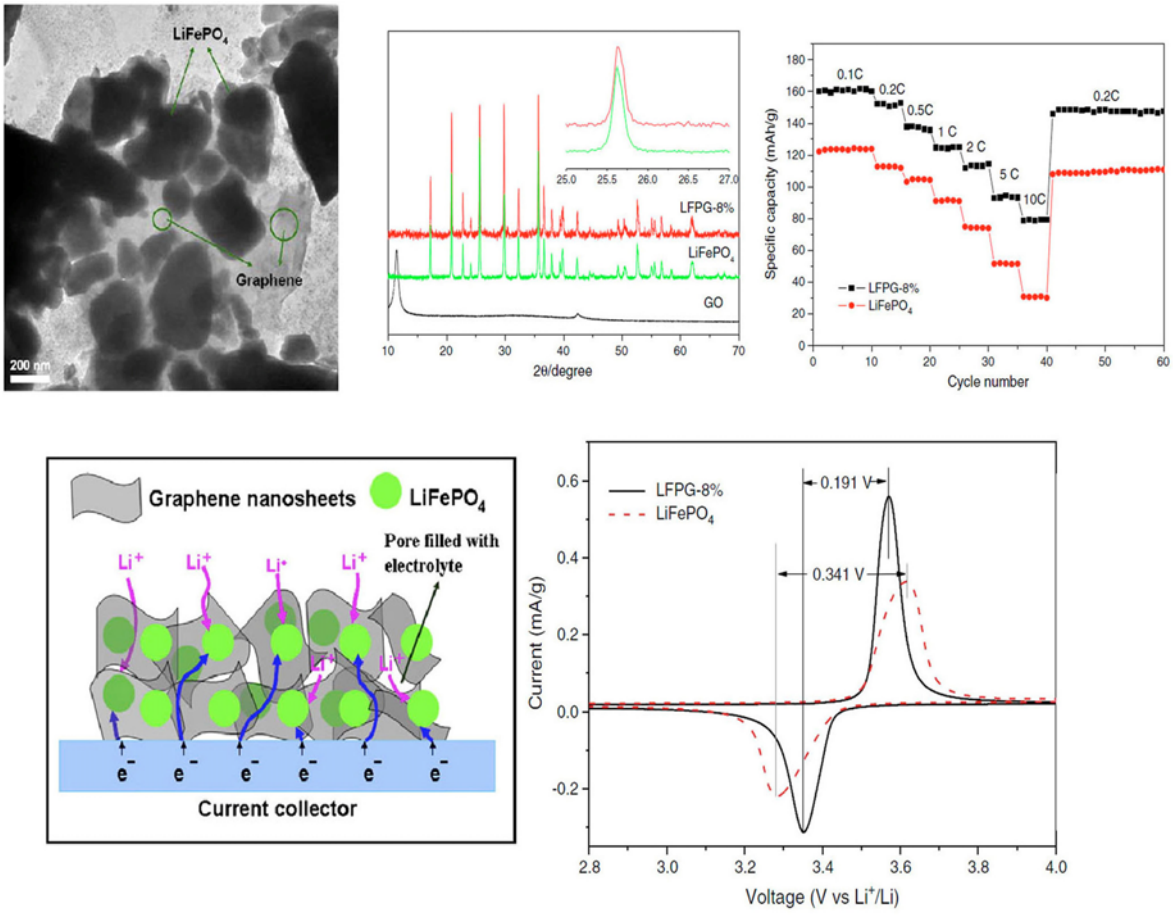

Fig. 16. TEM image, XRD pattern, rate performance and cyclic voltammogram of $LiFePO_4$-graphene nanocomposite.[107]

ble hydroxide and graphene oxide can be mixed at 450°C to precipitate Ni_6MnO_8 nanoparticles on larger reconstituted graphene sheets. This composition exhibited a capacity of 1030 $mAhg^{-1}$ during the first discharge and capacity of 400 $mAhg^{-1}$ after ten cycles.[109] As it is shown in Fig. 17, the precipitated graphene oxide/NiMn layered double hydroxide consists of large graphene oxide sheets on top of lamellar NiMn layered double hydroxide with smaller size. The interesting thing about this study was the use of temperature-dependent and the field dependence magnetization for the calcined graphene/NiMn. The nanocomposite showed fine room temperature paramagnetic properties. Magnetization saturation was estimated to be 9.4 and 21.8 $emug^{-1}$ for 300 and 2 K, respectively.

The study of the electrochemical behavior of the nanocomposite showed the reduction of the nanoparticles at the first discharge capacity of Ni_6MnO_8 can be declared by Eq. (27).[110,111]

$$Ni_6MnO_8 + (12 + x)Li \rightarrow 6Ni + 8Li_2O + Li_xMnO_2. \quad (28)$$

And the reversible charge/discharge can be stated by:

$$NiO + 2Li \leftrightarrow Ni + Li_2O. \quad (29)$$

As the industries demand lower price of preparation, the graphene/TiO_2 nanocomposites can be produced with water-based in situ precipitation method which is quite cheaper than other methods. In this technique, freshly prepared graphene oxides/TiO_2 can be obtained by precipitating $Ti(SO_4)_2$ with NH_3H_2O subjected to heat treatment in the presence of N_2.[112] The first discharge capacity of the nanocomposites showed an increase from 160 $mAhg^{-1}$ to 172 $mAhg^{-1}$. At the current density of 1 C, the capacity of the nanocomposite was 160 $mAhg^{-1}$ in the 1st cycle and 150 $mAhg^{-1}$ in the 10th cycle. At a current density of 3 C, the discharging capacity reduced to 140 $mAhg^{-1}$ and at the current density of 10 C, the discharge capacity was 110 $mAhg^{-1}$. The graphene/TiO_2 nanocomposites exhibited a high specific surface area of 125.5 m^2g^{-1}. Graphene-nickel oxide nanostructures are also the attractive anodes that can be synthesised by a controlled hydrothermal method, which enabled in situ formation of NiO with a coralloid nanostructure on graphene. This nanocomposite with 20 percent of NiO showed discharge capaci-

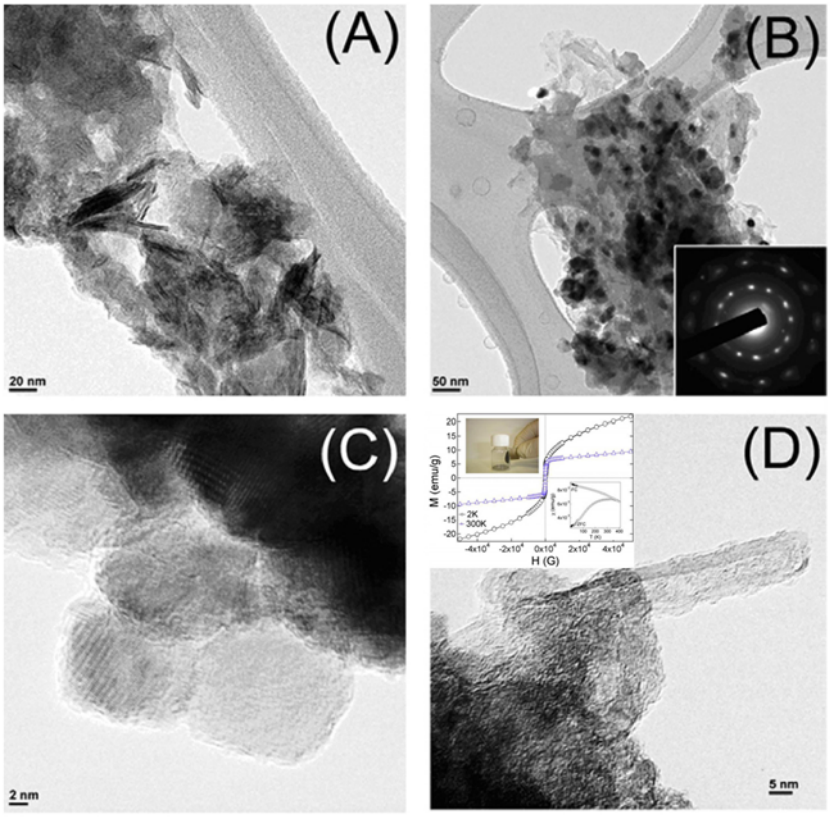

Fig. 17. (A) TEM of graphene oxide/NiMn layered double hydroxide, (B) graphene/NiMn layered double hydroxide, (C) high resolution of graphene/NiMn layered double hydroxide and (D) high resolution of graphene/NiMn layered double hydroxide with plate like NiMn.[109]

ties of 185 $mAhg^{-1}$ at 20 C, 450 $mAhg^{-1}$ at 1 C, and 400 $mAhg^{-1}$ at 1 C, respectively,[113] while when higher amount of NiO was used the graphene sheets were decorated by the in situ-formed NiO nanoparticles to form a film-like composite structure and the restacking of the graphene sheets was prevented.[114] In addition, potential application of α-MnO_2/graphene nanocomposites were investigated by synthesizing the nanocomposite in a facile wet-chemical route where α-MnO_2 nanosheets were uniformly distributed. The reversible capacity of the nanocomposite reported to be 726.5 $mAhg^{-1}$ at C/10 rate and 635.5 mA $h^{-1}g$ after 30 cycles. It was admitted that α-MnO_2 nanostructures prevents the pile of graphene nanosheets.[115] Si nanowires in graphene papers are the newly developed anodes that can be prepared by a supercritical fluid-liquid-solid process. The Si/graphene anode shoed reversible capacities of 1400 $mAhg^{-1}$ for the 30th cycle at a current density of 420 mAg^{-1}.[116] The reaction between Si nanoparticles and lithium during the charge transfer can be written as:

$$Si_{Crystal} \rightarrow Li_xSi_{Amorphous} \rightarrow Li_{15}Si_{4Crystal} \leftrightarrow Si_{Amorphous}. \quad (30)$$

First discharge capacity of 3506 $mAhg^{-1}$ and a subsequent charge capacity of 2009 $mAhg^{-1}$ has been achieved with Coulombic efficiency of 57.3%. Discharge capacity of 2227 $mAhg^{-1}$ was obtained in the second cycle and discharge capacity of 1386 $mAhg^{-1}$ was attained for the 30th cycle. The initial discharge capacity of the nanocomposite was 4080 $mAhg^{-1}$. The unique behavior of the nanocomposite can be associated with the graphene sheets as they can main-

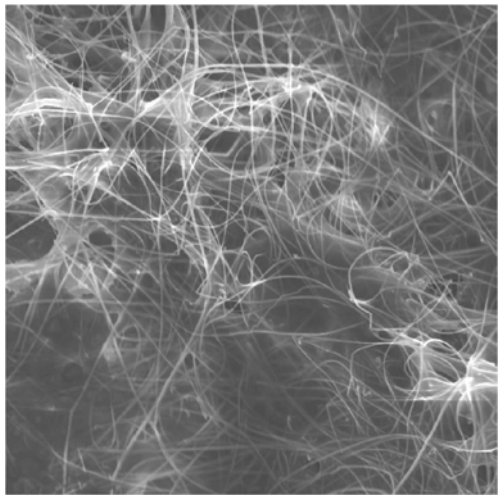

Fig. 18. Scanning electron microscope image of Si nanoparticle/graghene anode.[117]

tain the electrical contact between Si and the current collectors and absorption of volume changes of Si nanowries during the lithiation/delithiation (see Fig. 18).[117]

From another perspective, the diffusion of lithium in anode materials is the parameter which should be carefully investigated in future studies as its significant effect on the electrical properties of the lithium ion batteries cannot be neglected. The diffusion coefficient of lithium ions is dependent on the number of factors, which the amount of vacancies for hopping and concentration of lithium are the most important ones. The rate of hopping (λ) can be declared by the following equation:

$$\lambda = \nu^* \exp\left(\frac{-\Delta G}{kT}\right) \tag{31}$$

where ν^* is the vibration frequency and ΔG is the energy of activated barrier as a result of difference in activated state energy and initial equilibrium energy. The diffusion path in the structure of the nanocomposites highly depends on the local arrangement of lithium and vacancy around the endpoints of the hops, usually the shortest path between endpoints of the hops.[118,119] Using Devanathan-Stachurski electrochemical technique and ab initio computation, the diffusivity of lithium ions parallel to the graphene plane was found to be about 4.4×10^{-6} cm^2s^{-1} and the diffusivity of lithium ions along the grain boundaries of graphene was estimated to be around 10^{-12} cm^2s^{-1}.[120]

Graphite-like materials are the one which can be considered as the new generation of the anode graphines. This material can be prepared by high temperature treatment of carbon nanofiber by galvanostatic cycling. The graphitized carbon nano fiber showed reversible capacity of 320 $mAhg^{-1}$ after 50 cycles and cyclability and cycling efficiency of 99% as same as the values for oilderived graphite. The anode showed crystallinity and some loops between adjacent active end planes on the graphene layers.[121] From another view, lithium can be inserted into carbon-rich polymer-derived silicon oxycarbide nanocomposite by a thermal treatment at 400°C, 1100 and 1300°C. The nanocomposites prepared at 1100°C showed reversible capacity of 521 $mAhg^{-1}$ at a cycling current of 37 mAg^{-1}.[122] The main mechanism of lithium storage in Si-O-C based materials is the interstitial spaces between graphene layers, edges of graphene sheets and micropores as the major lithium storing sites.[123]

3. CONCLUSIONS

The current anode materials showed pulverization and cracking of electrode materials by volume change during charging and discharging, leading to a poor cycle performance. It is suggested that one dimensional nanowire materials or alloy-encapsulated hollow structures due to their stable mechanical structure can be used instead. From another point, graphene, a two-dimensional honeycomb of carbon atoms, is a rising star in the battery industry for its radical properties in terms of electrical conductivity and it can play a significant role in the development of anode nanocomposites. The ability of rechargeable lithium-ion batteries to store up to many times more energy than conventional designs is getting a boost thanks to a range of new conducting materials that doesn't break down after repeated usage. However, as there are tremendous researches in the area of developing lithium ion batteries especially on the progress of the anodes but considerable technical challenges are remained for commercializing the research products. There is a need to effectively produce nanocomposite anodes along with graphene that can complement the advantages of graphene while overcoming the drawbacks such as low capacities. To investigate the effect of structural changes Monte Carlo simulations are suggested.

With these motivations and objectives, it is expected to obtain a very high specific capacity and rate capabilities with high capacity retention after hundreds of repeated cycles for lithium-ion batteries based on graphene anode materials. In order to overcome some limitations such as low diffusivity, low electrical conductivity and structural instability, it is suggested to use conductive additives and nanowires and design the nanocomposite/graphite in strain graded architecture. Graphene sheets distributed between the nanoparticles can minimize the aggregation of the nanoparticles, the excellent electronic conductivity of graphene can facilitate electron transfer and mesoporous structure of the TiO_2-graphene nanocomposite provide short path length for both electron and lithium ion transports and large electrode/electrolyte contract area.

The majority of graphene/metal oxide materials were synthesized by mixing or dispersing their inorganic components with graphene, which leads to a weak interfacial interaction. A suitable indulgent of surface chemistry on graphene and metal oxides is critical for increasing interfacial interactions and achieving a uniform structure on graphene, by improving the surface chemistry using covalent or noncovalent techniques to enhance the charge transfer. The morphology of the metal matrix composites should be designed in a way that the electrical properties and stability of the anodes secured under thermal shocks. It is highly suggested that the nanocomposites should be improved using new nano materials like rare earth elements, new production routes as easier than the rest presented in this review, with the aim of reaching better electrochemical performance. It should be noted that there is still a need in understanding the thermodynamical and chemical reactions between the nanoparticles and graphene together with the concept of mechanisms of forming new phases during the processing of the graphene/nanocomposites. These finding might help to estimate the optimum size, microstructure and distribution of nanoparti-

cles. It is proposed though more work on the presence of thin-base oxides in the graphene structure can be helpful since it has been shown a great performance of this nanocomposite. In near future, the improved version of anodes might be helpful in the lithium ion batteries with a range of application in many electrical devices including laptops, smart phones, electrical vehicles and even the space machines where the critical point is the supply of energy. This is particularly important when the imagination of having flexible batteries can be easily achieved in a practical move by improving the graghene-based nanocomposites in the lithium ion batteries. In today's life, a better lithium-ion battery is demanded but if we think further, perhaps better solar, nuclear or fusion batteries would be the prospect view of green energy which it will be necessary to find a new source of energy that powers human-piloted spaceships.

REFERENCES

1. P. Simon and Y. Gogotsi, *Nature Mater.* **7**, 845 (2008).
2. H. Fukui, O. Hisashi, T. Hino, and K. Kanamura, *Appl. Mater. Interface* **2** 998 (2010).
3. Z.-S. Wu, G. Zhoua, L.-C. Yin, W. Ren, F. Li, and H.-M. Cheng, *Nano Energy* **1**, 107 (2012).
4. T. Takamura, K. Endo, L. Fu, and Y. Wu, *Electrochim. Acta* **53**, 1055 (2007).
5. J. P. Perdew, K. Burke, and M. Ernzerhof, *Phys. Rev. Lett.* **77**, 3865 (1996).
6. K. Tatsumi, N. Iwashita, H. Sakaebe, H. Shioyama, and S. Higuchi, *J. Electrochem. Soc.* **142**, 716 (1995).
7. L. J. Fu, H. Liu, C. Li, Y. P. Wu, E. Rahm, R. Holze, and H. Q. Wu, *Solid State Sci.* **8**, 113 (2006).
8. M. C. Smart, B. V. Ratnakumar, Jay F. Whitacre, L. D. Whitcanack, K. B. Chin, M. D. Rodreguez, D. Zhao, S. G. Greenbaum, and S. Surampudi, *J. Electrochem. Soc.* **152**, A1096 (2005).
9. Y. P. Wu, C. Jiang, C. Wan, and R. Holze, *Solid State Ionics* **156**, 283 (2003).
10 K. Tatsumia, T. Kawamurab, S. Higuchia, T. Hosotubob, H. Nakajimab, and Y. Sawada, *J. Power Sources* **68**, 263 (1997).
11. R. Hu, M. Zeng, C. Y. V. Li, and M. Zhu, *J. Power Source* **188**, 268 (2009).
12. K. Persson, Y. Hinuma, Y. Shirley Meng, A. Van der Ven, and G. Ceder, *Phys. Rev. B* **82**, 1 (2010).
13. S. W. Lee, N. Yabuuchi, B. M. Gallant, S. Chen, B.-S. Kim, P. T. Hammond, and Y. Shao-Horn, *Nature Nanotech.* **5**, 531 (2010).
14. S. Yang, X. Feng, L. Zhi, Q. Cao, J. Maier, and K. Müllen, *Adv Mat SI.: Carbon Mat.* **22**, 838 (2010).
15. J. S. Xue and J. R. Dahn, *J. Electrochem. Soc.* **142**, 3668 (1995).
16. J. Wang, J.-L. Liu, Y.-G Wang, C.-X. Wang, and Y.-Y. Xia, *Electrochim. Acta* **74**, 1 (2012).
17. M. Au, S. McWhorter, H. Ajo, T. Adams, Y. Zhao, and J. Gibbs, *J. Power Sources* **195**, 3333 (2010).
18. E. Kim, M. G. Kim, and J. Cho, *Electrochem. Solid St.* **9**, A311 (2006).
19. C. K. Chan, H. Peng, G. Liu, K. McIlwrath, X. F. Zhang, R. A. Huggins, and Y. Cui, *Nature Nanotech.* **3**, 31 (2008).
20. A. S. Aricò, P. Bruce, B. Scrosati, J.-M. Tarascon, and W. van Schalkwijk, *Nature Mat.* **4**, 366 (2005).
21. K. Tae Lee and J. Cho, *Nano Today* **6**, 28 (2011).
22. Y. Oumellal, A. Rougier, G. A. Nazri, J.-M. Tarascon, and L. Aymard, *Nature Mat.* **7**, 916 (2008).
23. J. R. Dahn, U. von Sacken, M. W. Juzkow, and H. AI Janaby, *J. Electrochem. Soc*. **138**, 2207 (1991).
24. E. V. Makhonina, V. S. Pervov, and V. S. Dubasova, *Chem. Rev*. **73**, 991 (2004).
25. R. Yazami, *J. Power Sources* **97-98**, 33 (2001).
26. R. Mukherjee, R. Krishnan, T.-M. Lu, and N. Koratkara, *Nano Energy* **1**, 518 (2012).
27. J. M. Tarascon and M. Armand, *Nature* **414**, 359 (2001).
28. S. Megahed and B. Scrosati, *J. Power Sources* **51**, 104 (1994).
29. S. J. Dillon and K. Sun, *Curr. Opin. Solid St M.* **16**, 153 (2012).
30. M. Endo, C. Kim, K. Nishimura, T. Fujino, and K. Miyashita, *Carbon* **38**, 183 (2000).
31. B. Scrosati, *Electrochim. Acta* **45**, 2461 (2000).
32. M. Endo, Y. Nishimura, T. Takahashi, K. Takeuchi, and M. S. Dresselhaus, *J. Phys. Chem. Solids* **57**, 725 (1996).
33. K. Kinoshita and K. Zaghib, *J. Power Sources* **110**, 1 (2002).
34. K. Sato, M. Noguchi, A. Demachi, N. Oki, and M. Endo, *Science* **264**, 5158 (1994).
35. G. W. Semenoff, *Phys. Rev. Lett*. **53**, 2449 (1984).
36. X. Huang, X. Qi, F. Boey, and H. Zhang, *Chem. Soc. Rev.* **41**, 666 (2012).
37. Z. Chen, M. Zhou, Y. Cao, X. Ai, H. Yang, and J. Liu, *Adv. Energy Mater.* **2**, 94 (2012).
38. C.-M. Park, S. Yoon, S.-I. Lee, and H.-J. Sohn, *J. Power Sources* **186**, 206 (2009).
39. K. Amine, I. Belharouak, Z. H. Chen, T. Tran, H. Yumoto, N. Ota, S. T. Myung, and Y. K. Sun, *Adv. Mater.* **22**, 3052 (2010).
40. L.-F. Cui, Y. Yang, C.-M. Hsu, and Y. Cui, *Nano Lett*. **9**, 3370 (2009).
41. J. Y. Luo, Y. G. Wang, H. M. Xiong, and Y. Y. Xia, *Chem. Mater.* **19**, 4791 (2007).
42. F. Badway, I. Plitz, S. Grugeon, S. Laruelle, M. Dolle, A. S. Gozdz, and J. M. Tarascon, *Electrochem Solid St.* **5**, A115 (2002).
43. K. T. Lee, Y. S. Jung, J. Y. Kwon, J. H. Kim, and S. M. Oh, *Chem. Mater.* **20**, 447 (2008).
44. Y. S. Jung, K. T. Lee, J. H. Kim, J. Y. Kwon, and S. M. Oh, *Adv. Funct. Mater.* **18**, 3010 (2008).

45. J. H. Ku, Y. S. Jung, K. T. Lee, C. H. Kim, and S. M. Oh, *J. Electrochem. Soc.* **156**, A688 (2009).
46. C. H. Kim, Y. S. Jung, K. T. Lee, J. H. Ku, and S. M. Oh, *Electrochim. Acta* **54**, 4371 (2009).
47. T. Bhardwaj, A. Antic, B. Pavan, V. Barone, and B. D. Fahlman, *J. Am. Chem. Soc*. **132**, 12556 (2010).
48. P. C. Lian, X. F. Zhu, S. Z. Liang, Z. Li, W. S. Yang, and H. H. Wang, *Electrochim. Acta* **55**, 3909 (2010).
49. H. Kim and J. Cho, *Nano Lett.* **8**, 3688 (2008).
50. C. Uthaisar and V. Barone, *Nano Lett*. **10**, 2838 (2010).
51. D. Zhao, Y. Wang, and Y. Zhang, *Nano-Micro Lett.* **3**, 162 (2011).
52. E. Pollak, B. S. Geng, K. J. Jeon, I. T. Lucas, T. J. Richardson, F. Wang, and R. Kostecki, *Nano Lett*. **10**, 3389 (2010).
53. E. Peled, C. Menachem, and A. Melman, *J. Electrochem. Soc.* **143**, L4 (1996).
54. S. Liang, X. Zhu, P. Lian, W. Yang, and H. Wang, *J. Solid State Chem.* **184**, 1400 (2011).
55. Y. Yu, C. H. Chen, and Y. Shi, *J. Adv. Mater.* **19**, 993 (2007).
56. X. Zhu, Y. Zhu, S. Murali, M. D. Stoller, and R. S. Ruoff, *J. Power Sources* **196**, 6473 (2011).
57. H. Liu, J. Huang, X. Li, J. Liu, Y. Zhang, and K. Du, *Appl. Surface Sci.* **258**, 4917 (2012).
58. M.-Y. Ma, Z.-Q. He, Z.-B. Xiao, K.-L. Huang, L.-Z. Xiong, and X.-M. Wu, *T. Nonferr. Metal. Soc.* **16**, 791 (2006).
59. S. H. Choi, J. S. Kim, and Y. S. Yoon, *Electrochim. Acta* **50**, 547 (2004).
60. R. K. Selvan, N. Kalaiselvi, C. O. Augustin, C. H. Doh, and C. Sanjeeviraja, *J. Power Sources* **157**, 522 (2006).
61. Y. Liang, J. Fan, X. Xia, Y. Luo, and Z. Jia, *Electrochim. Acta* **52**, 5891 (2007).
62. C. Li, W. Wei, S. Fang, H. Wang, Y. Zhang, Y. Gui, and R. Chen, *J. Power Sources* **195**, 2939 (2010).
63. D. W. Kim, I. S. Hwang, S. J. Kwon, H. Y. Kang, K. S. Park, Y. J. Choi, K. J. Choi, and J. G. Park, *Nano Lett*. **7**, 3041 (2007).
64. M. F. Hassan, M. M. Rahman, Z. Guo, Z. Chen, and H. Liu, *J. Mater. Chem*. **20**, 9707 (2010).
65. P. Lian, S. Liang, X. Zhu, W. Yang, and H. Wang, *Electrochim. Acta* **58**, 81 (2011).
66. S. M. Paek, E. Yoo, and I. Honma, *Nano Lett*. **9**, 72 (2009).
67. C. Zhang, X. Peng, Z. Guo, C. Cai, and Z. Chen, *Carbon* **50**, 1897 (2012).
68. V. C. Tung, Matthew J. Allen, Yang Yang, and Richard B. Kaner, *Nature Nanotech.* **4**, 25 (2009).
69. M. Zhang, D. Lei, X. Yin, L. Chen, Q. Li, Y. Wang, and T. Wang, *J. Mater. Chem*. **20**, 5538 (2010).
70. G. Zhou, D. W. Wang, F. Li, L. Zhang, N. Li, Z. S. Wu, L. Wen, G. Q. Lu, and H. M. Cheng, *Chem. Mater.* **22**, 5306 (2010).
71. P. Lian, X. Zhu, S. Liang, Z. Li, W. Yang, and H. Wang, *Electrochemical Acta* **56**, 4532 (2011).
72. J. Z. Wang, C. Zhong, D. Wexler, N. H. Idris, Z. X. Wang, L. Q. Chen, and H. K. Liu, *Chem. Eur. J.* **17**, 4661 (2011).
73. H. Xiang, B. Tian, P. Lian, Z. Li, and H. Wang, *J. Alloy. Compd.* **509**, 7205 (2011).
74. H. Xiang, K. Zhang, G. J. J. Yang Lee, C. Zou, X. Chen, and J. Wu, *Carbon* **49**, 1787 (2011).
75. H. Liu, J. Huang, X. Li, J. Liu, and Y. Zhang, *Ceram. Int.* **38**, 5145 (2012).
76. J. Lee, R. Zhang, and Z. Liu, *J. Power Sources* **90**, 70 (2000).
77. H. Momose, H. Honbo, S. Takeuchi, K. Nishimura, T. Horiba, Y. Muranaka, and Y. Kozono, *J. Power Sources* **68**, 208 (1997).
78. K. Nishimura, H. Honbo, S. Takeuchi, T. Horiba, M. Oda, M. Koseki, Y. Muranaka, Y. Kozono, and H. Miyadaera, *J. Power Sources* **68**, 436 (1997).
79. S. Kim, Y. Kadoma, H. Ikuta, Y. Uchimoto, and M. Wakihara, *Electrochem. Solid-State Lett.* **4**, A109 (2001).
80. T. Takamura, *Bull. Chem. Soc. Jpn.* **75**, 21 (2002).
81. Y. P. Wu, C. Wan, C. Jiang, and E. Tsuchida, *Electrochem. Comm.* **2**, 626 (2000).
82. Y. P. Wu, C. Jiang, C. Wan, and R. Holze, *J. Power Sources* **112**, 255 (2002).
83. X. Huang, X. Zhou, K. Qian, D. Zhao, Z. Liu, and C. Yu, *J. Alloy. Compd.* **514**, 76 (2012).
84. K. R. Kganyago and P. E. Ngoepe, *Phys. Rev. B.* **68**, 205111 (2003).
85. M. Choucair, Pall Thordarson, and John A. Stride, *Nature Nanotech.* **4**, 30 (2009).
86. M. Wagemaker, A. Van Der Ven, D. Morgan, G. Ceder, F. M. Mulder, and G. J. Kearley, *Chem. Phys.* **317**, 130 (2005).
87. G. Wang, J. Bai, Y. Wang, Z. Ren, and J. Bai, *Scripta Mater.* **65**, 339 (2011).
88. K. Chang, Z. Wang, G. Huang, H. Li, W. Chen, and J. Y. Lee, *J. Power Sources* **201**, 259 (2012).
89. D. Cai, P. Lian, X. Zhu, S. Liang, W. Yang, and H. Wang, *Electrochim. Acta* **74**, 65 (2012).
90. P. Guo, H. Song, X. Chen, L. Ma, G. Wang, and F. Wang, *Anal. Chim. Acta* **688**, 146 (2011).
91. H. Kim, D. H. Seo, S. W. Kim, J. Kim, and K. Kang, *Carbon* **49**, 326 (2011).
92. Y. J. Mai, S. J. Shi, D. Zhang, Y. Lu, C. D. Gu, and J. P. Tu, *J. Power Sources* **204**, 155 (2012).
93. C.-T. Hsieh, C.-Y. Lin, and J.-Y. Lin, *Electrochim. Acta* **56**, 8861 (2011).
94. H.-C. Tao, L.-Z. Fan, Y. Mei, X. Q.-C. Tao, L.-Z. Fan, Y. Mei, and X. Qu, *J. Power Sources* **202**, 230 (2012).
95. J. Z. Wang, C. Zhong, S. L. Chou, and H. K. Liu, *Electrochem. Commun*. **12**, 1467 (2010).
96. P. C. Lian, X. F. Zhu, S. Z. Liang, Z. Li, W. S. Yang, and H. H. Wang, *Electrochim Acta* **55**, 3909 (2010).

97. K.-H. Kim, D.-W. Jung, V. H. Pham, J. S. Chung, B.-S. Kong, J. K. Lee, K. Kim, and E.-S. Oh, *Electrochim. Acta* **69**, 358 (2012).
98. H. Kim, D.-H. Seo, S.-W. Kim, J. Kim, and K. Kang, *Carbon* **49**, 326 (2011).
99. L. Tao, J. Zai, K. Wang, H. Zhang, M. Xu, J. Shen, Y. Su, and X. Qian, *J. Power Sources* **202**, 230 (2012).
100. X. Wang, X. Zhou, K. Yao, J. Zhang, and Z. Liu, *Carbon* **49**, 33 (2011).
101. A. Bhaskara, M. Deepaa, T. N. Raob, and U. V. Varadaraju, *J. Power Sources* **216**, 169 (2012).
102. J. K. Lee, K. B. Smith, C. M. Hayner, and H. H. Kung, *Chem. Commun*. **46**, 2025 (2010).
103. X. Zhou, Y.-X. Yin, L.-J. Wan, and Y.-G. Guo, *Chem. Commun.* **48**, 2198 (2012).
104. J.-Z. Wang, C. Zhong, S.-L. Chou, and H.-K. Liu, *Electrochem. Commun.* **12**, 1467 (2010).
105. J. Xie, Y.-X. Zheng, R.-J. Pan, S.-Y. Liu, W.-T. Song, G.-S. Cao, T.-J. Zhu, and X.-B. Zhao, *Int. J. Electrochem. Sci*. **6**, 4811 (2011).
106. A. K. Padhi, K. S. Nanjundaswamy, and J. B. Goodenough, *J. Electrochem. Soc*. **144**, 1188 (1997).
107. L. Wang, H. Wang, Z. Liu, C. Xiao, S. Dong, P. Han, Z. Zhang, X. Zhang, C. Bi, and G. Cui, *Solid State Ionics* **181**, 1685 (2010).
108. Z. S. Wu, W. C. Ren, L. Wen, L. B. Gao, J. P. Zhao, Z. P. Chen, G. M. Zhou, F. Li, and H. M. Cheng, *ACS Nano.* **4**, 3187 (2010).
109. Marcos Latorre-Sanchez, Pedro Atienzar, Gonzalo Abellán, Marta Puche, Vicente Fornés, Antonio Ribera, and Hermenegildo García, *Carbon* **50**, 518 (2012).
110. R. Alca´ntara, M. Jaraba, P. Lavela, and J. L. Tirad, *J. Solid State Chem*. **166**, 330 (2002).
111. S. S. Kim, S. Ogura, H. Ikuta, Y. Unchimoto, and M. Wakihara, *Solid State Ionics* **146**, 249 (2002).
112. Y.-H. Ding, P. Zhang, H.-M. Ren, Q. Zhuo, Z.-M. Yang, and Y. Jiang, *Mater. Res. Bull.* **46**, 2403 (2011).
113. Iresha R.M. Kottegoda, Nurul Hayati Idris, Lin Lu, Jia-Zhao Wang, and Hua-Kun Liu, *Electrochim. Acta* **56**, 5815 (2011).
114. Z. Ji, J. Wu, X. Shen, H. Zhou, and H. Xi, *J. Mater. Sci.* **46**, 1190 (2011).
115. L. Xing, C. Cui, C. Ma, and X. Xue, *Mater. Lett.* **65**, 2104 (2011).
116. Z. Lu, J. Zhu, D. Sim, W. Shi, Y. Y. Tay, J. Ma, H. H. Hng, and Q. Yan, *Electrochim. Acta* **74**, 176 (2012).
117. J. C. Guo, A. Sun, X. L. Chen, C. S. Wang, and A. Manivannan, *Electrochim. Acta* **56**, 3981 (2011).
118. A. Van der Ven and G. Ceder, *J. Power Sources* **97-98**, 529 (2001).
119. B. Kang and G. Ceder, *Nature* **458**, 190 (2009).
120. K. Persson, V. A. Sethuraman, L. J. Hardwick, Y. Hinuma, Y. S. Meng, A. van der Ven, V. Srinivasan, R. Kostecki, and G. Ceder, *J. Phys. Chem. Lett.* **1**, 1176 (2010).
121. I. Cameán, A. B. García, I. Suelves, J. L. Pinilla, M. J. Lázaro, and R. Moliner, *J. Power Sources* **198**, 303 (2012).
122. J. Kaspar, M. Graczyk-Zajac, and R. Riedel, *Solid State Ionics* **225**, 527 (2012).
123. B. Scrosati, *Electrochim. Acta* **45**, 2461 (2000).